

การคำนวณทางเคมีเชิงคอมพิวเตอร์ของผลของโครงสร้างและการแพร่ของอีเทนและไนโตรเจนใน  
โครงข่ายโพลีเอทิลีนกึ่งผลึก-8



นางสาวตติยา โชคบุญเปี่ยม

จุฬาลงกรณ์มหาวิทยาลัย

CHULALONGKORN UNIVERSITY

วิทยานิพนธ์นี้เป็นส่วนหนึ่งของการศึกษาตามหลักสูตรปริญญาวิทยาศาสตรดุษฎีบัณฑิต

สาขาวิชาปิโตรเคมี

คณะวิทยาศาสตร์ จุฬาลงกรณ์มหาวิทยาลัย

ปีการศึกษา 2556

ลิขสิทธิ์ของจุฬาลงกรณ์มหาวิทยาลัย

บทคัดย่อและแฟ้มข้อมูลฉบับเต็มของวิทยานิพนธ์ตั้งแต่ปีการศึกษา 2554 ที่ให้บริการในคลังปัญญาจุฬาฯ (CUIR)

เป็นแฟ้มข้อมูลของนิสิตเจ้าของวิทยานิพนธ์ ที่ส่งผ่านทางบัณฑิตวิทยาลัย

The abstract and full text of theses from the academic year 2011 in Chulalongkorn University Intellectual Repository (CUIR) are the thesis authors' files submitted through the University Graduate School.

COMPUTATIONAL CHEMISTRY CALCULATIONS OF STRUCTURE EFFECTS AND  
DIFFUSION OF ETHANE AND NITROGEN IN ZEOLITIC IMIDAZOLATE FRAMEWORK-8



Miss Tatiya Chokbunpiam

จุฬาลงกรณ์มหาวิทยาลัย

**CHULALONGKORN UNIVERSITY**

A Dissertation Submitted in Partial Fulfillment of the Requirements  
for the Degree of Doctor of Philosophy Program in Petrochemistry

Faculty of Science

Chulalongkorn University

Academic Year 2013

Copyright of Chulalongkorn University

Thesis Title	COMPUTATIONAL CHEMISTRY CALCULATIONS OF STRUCTURE EFFECTS AND DIFFUSION OF ETHANE AND NITROGEN IN ZEOLITIC IMIDAZOLATE FRAMEWORK-8
By	Miss Tatiya Chokbunpiam
Field of Study	Petrochemistry
Thesis Advisor	Professor Supot Hannongbua, Dr.rer.nat.
Thesis Co-Advisor	Rungroj Chanajaree, Dr.rer.nat. Siegfried Fritzsche, Priv-Doz.Dr.rer.nat.habil.

---

Accepted by the Faculty of Science, Chulalongkorn University in Partial  
Fulfillment of the Requirements for the Doctoral Degree

.....Dean of the Faculty of Science  
(Professor Supot Hannongbua, Dr.rer.nat.)

THESIS COMMITTEE

.....Chairman  
(Professor Pattarapan Prasassarakich, Ph.D.)

.....Thesis Advisor  
(Professor Supot Hannongbua, Dr.rer.nat.)

.....Thesis Co-Advisor  
(Rungroj Chanajaree, Dr.rer.nat.)

.....Thesis Co-Advisor  
(Siegfried Fritzsche, Priv-Doz.Dr.rer.nat.habil.)

.....Examiner  
(Assistant Professor Somsak Pianwanit, Ph.D.)

.....Examiner  
(Duangamol Tungasmita, Ph.D.)

.....External Examiner  
(Oraphan Saengsawang, Dr.rer.nat.)

ตติยา โขคบุญเปี่ยม : การคำนวณทางเคมีเชิงคอมพิวเตอร์ของผลของโครงสร้างและการแพร่ของอีเทนและไนโตรเจนในโครงข่ายซีโอไลติกอิมิดาโซเลต-8. (COMPUTATIONAL CHEMISTRY CALCULATIONS OF STRUCTURE EFFECTS AND DIFFUSION OF ETHANE AND NITROGEN IN ZEOLITIC IMIDAZOLATE FRAMEWORK-8) อ.ที่ปรึกษาวิทยานิพนธ์หลัก: ศ. ดร. สุพจน์ หารหนองบัว, อ.ที่ปรึกษาวิทยานิพนธ์ร่วม: ดร. รุ่งโรจน์ ฆานะจारी, ดร. Siegfried Fritzsche, 82 หน้า.

โครงข่ายซีโอไลติกอิมิดาโซเลต-8 (ซีฟ-8) วัสดุพรุนที่ได้รับความสนใจอย่างกว้างขวาง เนื่องจากมันมีเสถียรภาพสูงต่อสารเคมีและความร้อน ในงานนี้ได้ศึกษาเปรียบเทียบชุดพารามิเตอร์ต่างๆ สำหรับอันตรกิริยาระหว่างโมเลกุลของซีฟ-8 รวมถึงเกสต์โมเลกุล โดยเปรียบเทียบผลจากการจำลองพลวัตเชิงโมเลกุลกับการทดลอง จากการเลือกใช้ชุดพารามิเตอร์ที่เหมาะสม ได้ทำการศึกษาการแพร่ของโมเลกุลอีเทนและไนโตรเจนรวมถึงผลกระทบของการแพร่ของโมเลกุลที่มีต่อขนาดของหน้าต่าง สำหรับอีเทนพบผลกระทบสองอย่างที่ที่น่าสนใจ เมื่อปริมาณของอีเทนสูงขึ้น ขนาดของหน้าต่างจะเล็กลงและแรงที่ผลักดันโมเลกุลไปทางหน้าต่าง ผลกระทบทั้งสองนี้ถ่วงดุลซึ่งกันและกัน ทำให้ค่าการแพร่แทบจะไม่ขึ้นกับความเข้มข้นของอีเทน สำหรับไนโตรเจนนั้นพบผลกระทบประตูเปิด ซึ่งผลนี้สอดคล้องกับการทดลอง ขนาดของหน้าต่างใหญ่ขึ้นที่ความเข้มข้นสูง แต่ในขณะเดียวกันไม่ได้ทำให้การแพร่ของไนโตรเจนสูงขึ้น อันตรกิริยาที่ซับซ้อนของโฮสต์-โฮสต์ และโฮสต์-เกสต์ มีผลทำให้โมเลกุลไนโตรเจนกีดขวางซึ่งกันและกัน และถ่วงดุลความเร็วของการเคลื่อนที่เนื่องจากขนาดหน้าต่างที่ใหญ่ขึ้น นอกจากนี้ได้ศึกษาค่าพลังงานกีดขวางสำหรับการหมุนของตัวเชื่อมอิมิดาโซเลตโดยวิธีทางกลศาสตร์ควอนตัม ผลที่ได้แสดงถึงพลังงานกระตุ้นที่สูงมากประมาณ 200 kcal/mol สำหรับปรากฏการณ์ประตูเปิด

จุฬาลงกรณ์มหาวิทยาลัย

CHULALONGKORN UNIVERSITY

สาขาวิชา ปีโตรเคมี

ปีการศึกษา 2556

ลายมือชื่อนิสิต .....

ลายมือชื่อ อ.ที่ปรึกษาวิทยานิพนธ์หลัก .....

ลายมือชื่อ อ.ที่ปรึกษาวิทยานิพนธ์ร่วม .....

ลายมือชื่อ อ.ที่ปรึกษาวิทยานิพนธ์ร่วม .....

# # 5273813523 : MAJOR PETROCHEMISTRY

KEYWORDS: COMPUTATIONAL CHEMISTRY CALCULATIONS / ADSORPTION /  
DIFFUSION / ETHANE AND NITROGEN IN ZIF-8.

TATIYA CHOKBUNPIAM: COMPUTATIONAL CHEMISTRY CALCULATIONS OF  
STRUCTURE EFFECTS AND DIFFUSION OF ETHANE AND NITROGEN IN  
ZEOLITIC IMIDAZOLATE FRAMEWORK-8. ADVISOR: PROF. SUPOT  
HANNONGBUA, Dr.rer.nat., RUNGROJ CHANAJAREE, Dr.rer.nat., SIEGFRIED  
FRITZSCHE, Priv-Doz.Dr.rer.nat.habil., 82 pp.

Zeolitic Imidazolate Framework-8 (ZIF-8), a porous material, has attracted great attention due to its high chemical and thermal stability. In this work the applicability of parameter sets for the molecular interactions of ZIF-8 including guest molecules was investigated by comparing results of MD simulations with experiments. Using suitable parameter sets, the diffusion and the effect of the diffusing molecules on the window size were investigated for ethane and nitrogen. For ethane, two interesting effects were found at higher ethane loadings: reduction of the window size and, forces that push a given molecule toward the window. These two effects balance each other leading to a self-diffusivity nearly independent upon the concentration of ethane. For nitrogen a gate-opening effect could be found. This result is in agreement with experiments. The size of the windows increases at high loadings while this does not speed-up the nitrogen self-diffusivity. The complex interactions of host-host and host-guest molecules cause mutual hindrance of the nitrogen molecules and balance the speed of the mobility due to the larger window size. Moreover, the energy barrier for rotation of imidazolate linkers was studied by quantum mechanics (QM). The results show a very large activation energy about 200 kcal/mol for gate-opening phenomena.

Field of Study: Petrochemistry

Academic Year: 2013

Student's Signature .....

Advisor's Signature .....

Co-Advisor's Signature .....

Co-Advisor's Signature .....

## ACKNOWLEDGEMENTS

This dissertation would not be possible and workable without people who supported and encouraged me. Therefore, in this acknowledgment I would like to declare and thank the people that have collaborated in my work.

Firstly, I would like to appreciatively thank my advisor Prof. Dr. Supot Hannongbua and also my co-advisors consist of Priv-Doz. Dr. Siegfried Fritzsche and Dr. Rungroj Chanajaree for giving me the chance to study at Chulalongkorn University and do the research at Leipzig University such a great places where I was able to learn and to apply my Doctor of Philosophy Program under their kind suggestion and constant help.

I would like to take this opportunity to thank Assoc. Prof. Dr. Vudhichai Parasuk, Asst. Prof. Dr. Tawun Remsungnen and Dr. Piti Treesukol for several nice suggestions, discussion and cheer me up in hard time. Furthermore, I would like to thank Prof. Dr. Pattarapan Prasassarakich, Asst. Prof. Dr. Somsak Pianwanit, Dr. Oraphan Saengsawang, and Dr. Duangamol Tungasmita, who act as the thesis committee. Special thanks go to my family and my friends such as Tanawat Ploymeerusmee and Uthumporn Arsawang, who supported me throughout this work. Their unconditional love is the source of my power.

Lastly, I also would like to acknowledge the Commission of Higher Education for the Sandwich Ph.D. Program (CHE-PHD-SW) scholarship, Ratchadaphiseksomphot Endowment Fund of Chulalongkorn University (RES560530184-AM) and Petroleum, Petrochemicals, and Advanced Materials are gratefully acknowledged for financial supporting. All facilities and computer resources are offered by the Computational Chemistry Unit Cell (CCUC) at Department of Chemistry, Faculty of Science, Chulalongkorn University, Molecular Dynamics/Computer simulation (MDC) unit, the computer center of Leipzig University and the center for information services and high performance computing (ZIH) of Dresden University of Technology.

## CONTENTS

	Page
THAI ABSTRACT .....	iv
ENGLISH ABSTRACT .....	v
ACKNOWLEDGEMENTS .....	vi
CONTENTS .....	vii
LIST OF TABLES .....	x
LIST OF FIGURES .....	xi
LIST OF ABBREVIATIONS .....	xiv
CHAPTER I INTRODUCTION .....	1
1.1 Research rationale .....	1
1.2 Zeolitic Imidazolate Frameworks (ZIFs) .....	2
1.3 Applications.....	3
1.3.1 Gas storage .....	4
1.3.2 Gas separation .....	4
1.3.3 Catalysis .....	4
1.3.4 Drug delivery .....	5
1.4 Zeolitic Imidazolate Framework-8 (ZIF-8).....	5
1.5 Literature reviews .....	6
1.6 Scope of this study.....	8
CHAPTER II THEORY BACKGROUND .....	10
2.1 Molecular dynamics simulations .....	10
2.1.1 Classical mechanics.....	11
2.1.2 Integration algorithms .....	12
2.1.3 Force field .....	14
2.1.3.1 Intramolecular potential .....	14
2.1.3.2 Intermolecular potential.....	16
2.1.4 Periodic Boundary Conditions .....	18
2.1.5 Ensembles .....	19

	Page
2.1.6 Principle of diffusion .....	20
2.1.6.1 Transport diffusion .....	20
2.1.6.2 Self-diffusion .....	21
2.1.7 Radial distribution function.....	22
2.2 Quantum chemistry.....	24
2.2.1 The Schrödinger equation.....	24
2.2.2 Born-Oppenheimer approximation .....	25
2.2.3 Hartree-Fock approximation.....	26
2.2.4 LCAO approximation .....	27
2.2.5 Density functional theory.....	27
2.2.6 Basis set .....	28
2.2.6.1 Effective core potential.....	29
CHAPTER III CALCULATION DETAILS.....	30
3.1 Molecular dynamics (MD) simulations.....	30
3.1.1 General features of the simulations .....	30
3.1.2 Force field validation using isothermal-isobaric (NPT) ensemble.....	31
3.1.3 Dynamic properties of ethane molecules in ZIF-8 framework with different interactions.....	32
3.1.4 Potential energy profile for an ethane molecule passing the window.....	33
3.1.5 Structure of the flexible ZIF-8 framework and dynamic properties of N <sub>2</sub> within ZIF-8 framework with various interactions.....	34
3.2 Quantum chemical calculations.....	35
CHAPTER IV RESULTS AND DISCUSSION .....	37
4.1 Molecular dynamics (MD) simulations for C <sub>2</sub> H <sub>6</sub> .....	37
4.1.1 Framework properties for different force fields .....	37
4.1.2 C <sub>2</sub> H <sub>6</sub> diffusivity in ZIF-8 framework.....	39
4.1.3 Influence of the concentration of C <sub>2</sub> H <sub>6</sub> on the self-diffusion coefficient and the windows size .....	41



	Page
4.1.4 The potential threshold in the window.....	43
4.2 Molecular dynamics (MD) simulations for N <sub>2</sub> .....	45
4.2.1 Force field validation for the flexible ZIF-8 framework at 258 K and 300K by NPT ensemble .....	46
4.2.2 Force field validation for the flexible ZIF-8 framework with N <sub>2</sub> loading at 300K by NPT ensemble .....	47
4.2.3 Flexible ZIF-8 framework and N <sub>2</sub> dynamics investigated in the NVE ensemble.....	48
4.2.4 More detailed examination of the gate-opening effect .....	52
4.3 Quantum chemical calculations.....	58
CHAPTER V CONCLUSIONS .....	61
REFERENCES .....	63
APPENDIX.....	69
APPENDIX A Interaction parameters for the flexible models of ZIF-8 framework, C <sub>2</sub> H <sub>6</sub> , N <sub>2</sub> and the procedure of evaluating the window diameter.....	70
APPENDIX B The self-diffusion coefficients for C <sub>2</sub> H <sub>6</sub> and N <sub>2</sub> in ZIF-8 framework. ....	79
VITA.....	82

## LIST OF TABLES

Table 4.1 The edge lengths of the MD boxes and the Zn-N bond lengths of ZIF-8 found in the MD simulations with NPT ensemble with the different parameter sets, respectively and differences from the XRD derived structure (box size: 33.982 Å and Zn-N bond: 1.987 Å). Note that the box lengths in x, y, and z directions are equal. The deviations from experimental XRD values are written in parenthesis.....38



## LIST OF FIGURES

Figure 1.1 The bridging angles in ZIFs and zeolites structures: 1 is ZIF. 2 is zeolite [8].	2
Figure 1.2 The single crystal x-ray structures of ZIFs were shown in left and center columns. The largest cage in each ZIF was shown in right column [8].	3
Figure 1.3 The single crystal X-ray structures of ZIF-8 that consists of Zn cluster and MeIM linker [8].	5
Figure 2.1 The bonded potential; (a) The bond-stretching potential. (b) The angle bending potential. (c) The torsional potential (also called dihedral potential).	15
Figure 2.2 Van Der Waals interaction between two atoms including repulsive and attractive forces.	16
Figure 2.3 Electrostatic interaction between a pair of atoms.	17
Figure 2.4 Electrostatic interaction between a pair of atoms.	18
Figure 2.5 (a) Graphic of the particles in a simple atomic liquid and (b) schematic example of a radial distribution function as it could result from a simulation.	23
Figure 3.1 ZIF-8 structure. The 2x2x2 unit cells (left) and the 6-membered pore aperture with six 2 methyl-imidazolate linkers and six Zn <sup>2+</sup> ions (right).	31
Figure 3.2 The 6-membered window of the ZIF-8 framework as estimated from XRD data [8] plus adding the hydrogen electron clouds which gives a diameter of 3.4 Å. A yellow sphere is visualizing the window size.	33
Figure 3.3 The arrangement used for the molecular mechanics (a) top view, (b) side view. The dumbbell represents the C <sub>2</sub> H <sub>6</sub> molecule.	34
Figure 3.4 Different views of the part of 4-membered ring in the ZIF-8 lattice that formed the model for the quantum mechanical calculations.	35
Figure 3.5 Different views of the model part of 6-membered ring used in the quantum mechanical evaluations.	36
Figure 4.1 Potential (U <sub>bond</sub> ) for the vibration of the Zn-N bond (harmonic oscillator) calculated from the force field parameters used from refs [19] and [35].	37

Figure 4.2 (Left) The mean square displacements (MSDs) of $C_2H_6$ molecules in ZIF-8 at loading of 2.5 molecules/cage and the obtained self-diffusion coefficients ( $D_s$ ) for system A (a), system B (b), system C (c), and systems D and E (d). (Right) The distributions of the window diameters from the simulations of 2.5 molecules/cage for all parameter sets.....	40
Figure 4.3 Superimpositions of the 6-membered ring from XRD (black) and that from the simulations of ZIF-8 lattice with $C_2H_6$ molecules (red) for the parameter sets A (left) and D (right).....	41
Figure 4.4 $D_s$ for $C_2H_6$ in a ZIF-8 for the parameter sets A and C as function of loading (see appendix B in Table B.1) compared with experimental results. $D_s$ values from IRM are calculated from DT values as expressed in [71]. .....	41
Figure 4.5 (a) Windows diameter distributions as function of loadings with $C_2H_6$ achieved from the sets A and C (the results for the parameter sets A and C are nearly the same). (b) Average window diameters gained from snapshots from trajectories from parameter set C. ....	42
Figure 4.6 The energy barriers for $C_2H_6$ molecule obtained as described in the text for parameter sets A, C and D (see in Figure 4.2 right). The loading was 2.5 guest molecules/cage at 300 K. Note, the inlets shall only demonstrate the geometry of the arrangement and do not represent the real atom sizes. ....	44
Figure 4.7 The potential energy profile for $C_2H_6$ probe molecule passing the ZIF-8 window for the parameter set C at a loading of 15 molecules/cage at 300 K. The states are selected randomly from one trajectory in which no other $C_2H_6$ is within the window region.....	45
Figure 4.8 The box size distributions of ZIF-8 framework at 258 K and 300 K achieved from the MD simulations under the NPT ensemble (a) Parameter set C and (b) Parameter set F.....	46
Figure 4.9 The box length distributions of ZIF-8 within $N_2$ loading at 300 K acquired from the MD simulations under the NPT ensemble with (a) Parameter set C and (b) Parameter set F.....	48
Figure 4.10 Distributions of ZIF-8 window diameters at 258 K and 300 K for parameter sets C and F. ....	49

Figure 4.11 (a) Window diameters and (b) self-diffusivity $D_s$ (see in appendix B in Table B.2) for $N_2$ molecules within ZIF-8 framework for the parameter sets C and F.	50
Figure 4.12 Distributions of ZIF-8 window diameters for different $N_2$ loadings at 300 K for parameter set C. (a) $N_2$ loading from 0.5-18.44 molecules/cage (b) $N_2$ loading from 20.0-30.0 molecules/cage.	51
Figure 4.13 The transform of the orientation of the imidazolate linkers in the ZIF-8 framework for (a) low density (0.5 $N_2$ /cage) and (b) high density (15.0 $N_2$ /cage) $N_2$ loadings. Superimpositions of the low loading (black) and high loading (red) structures are shown for (c) the 4-membered ring and (d) the 6-membered ring.	53
Figure 4.14 Comparison of the probability density plots for $N_2$ and $C_2H_6$ molecules at different loadings in ZIF-8. In each column the left hand picture shows a larger area whereas right hand picture shows the projection of a single cavity centered in the picture. Dark regions signify high probability density.	54
Figure 4.15 RDFs for a $N_2$ molecule around the CC, CR, CT and Zn atoms in ZIF-8 framework at (a) 2.5 $N_2$ , (b) 7.5 $N_2$ (c) 12.5 $N_2$ , (d) 18.44 $N_2$ , (e) 24.69 $N_2$ and (f) 30.0 $N_2$ /cage.	55
Figure 4.16 RDF between N-N atoms for a $N_2$ molecule at different loadings in ZIF-8 framework.	56
Figure 4.17 The relative energy (kcal/mol) obtained from the quantum chemical calculations for the ZIF-8 linkers turning in the 4-membered ring in the ranges $0^\circ$ - $360^\circ$ (a) and $0^\circ$ - $30^\circ$ (b), and 6-membered ring in the ranges $0^\circ$ - $360^\circ$ (c).	58
Figure 4.18 (a) Structures of 4-membered ring and (b) 6-membered ring.	59

## LIST OF ABBREVIATIONS

AO	=	Atomic orbital
Å	=	Angstrom
$a_i$	=	acceleration of atom $i$
B3LYP	=	Beck's three parameter hybrid functional using the LYP correlation function
C	=	Concentration
$C^*$	=	Number density of labeled particle
D	=	Diffusion constant
$D_s$	=	Self-diffusion constant
$D_t$	=	Transport diffusion coefficient
DZ	=	Double zeta
DFT	=	Density functional theory
E	=	Energy
$E^{el}$	=	Electronic energy
ECP	=	Effective core potential
$F_i$	=	Total force of atom $i$
$g(r)$	=	Probability of finding atom at distance of $r$
HF	=	Hatree-Fock
$\hat{H}$	=	Hamiltonian operator
$J$	=	Flux density
kcal/mol	=	Kilocalorie per mole
KS	=	Kohn-Sham
$k_b$	=	Boltzmann constant
$k_r$	=	Force constant of bond
$k_\theta$	=	Force constant of bending angle
$k_\phi$	=	Force constant of torsional rotation
KS	=	Kohn-Sham
$L$	=	Onsager coefficient
LCAO	=	Linear combination of atomic orbital
LYP	=	Lee-Yang-Parr functional
$M_A$	=	Proportion of mass of nucleus A
MO	=	Molecular orbital
$m_i$	=	mass of atom $i$
$N$	=	Particles from the trajectory

$n(r)$	=	Ratio of local density
$N(r, \Delta r)$	=	Number of atoms a spherical shell of radius $r$ and thickness $\Delta r$
NVE	=	Microcanonical ensemble
NVT	=	Canonical Ensemble
NPT	=	Isobaric-Isothermal Ensemble
P	=	Pressure
$P_i$	=	Possibility of atom $i$
QM	=	Quantum mechanics
$q_i$	=	Partial charge of atom $i$
$q_j$	=	Partial charge of atom $j$
$r_0$	=	Equilibrium value of bond lengths
$r_{ij}$	=	Actual distance atoms
$\Delta r$	=	Volume of spherical shell with thickness
$\vec{r}_i$	=	Position of atom $i$
$\vec{r}_j$	=	Position of atom $j$
$\vec{r}^j(t)$	=	Position of molecule $i$ at time
RDF	=	Radial distribution function
SCF	=	Self-consistent field
$t$	=	Time
T	=	Temperature
$U$	=	Potential energy
$U_{total}$	=	Total potential energy
$U_{bonded}$	=	Intramolecular potential or bonded potential
$U_{non-bonded}$	=	Intermolecular potential or non-bonded potential
$U_{bond}$	=	Bond-stretching potential energy
$U_{angle}$	=	Angle-bending potential energy
$U_{torsion}$	=	Torsion potential energy
$U_{Van Der Waals}$	=	Van Der potential energy
$U_{electrostatic}$	=	Electrostatic potential energy
$\mu$	=	Chemical potential
V	=	Volume
$v$	=	Velocity
$\vec{v}_{i0}$	=	Initial velocity of atom $i$
$V_{eff}$	=	Effective potential

$v_x$	=	Velocity in x direction
$W$	=	Probability density
$x_0$	=	Initial position
$x$	=	Position
$Z$	=	Nuclear charge
$\theta_0$	=	Ideal angle
$\theta_{ijk}$	=	Equilibrium value of bond angle
$\phi$	=	Basis function
$\phi_0$	=	Ideal torsional rotation
$\phi_{ijkl}$	=	Equilibrium value of torsional rotation
$\epsilon_0$	=	Effective dielectric function
$\epsilon_{ij}$	=	Minimum of potential for interaction
$\sigma_{ij}$	=	Collision diameter or LJ diameter
$\Psi$	=	Function of the electron coordinates
$\chi$	=	Spin orbital
$\delta(x)$	=	Delta function
$\nabla^2$	=	Laplacian



# CHAPTER I

## INTRODUCTION

### 1.1 Research rationale

Porous materials have power for applications in several industrial processes to be employed for energetic resources and environment protection in terms of gas adsorption, gas separation and catalysis [1-4]. As promising candidates to accomplish these requirements, porous material such as zeolites have attracted attention for many decades. New porous materials, called Metal-Organic Frameworks (MOFs), can be created by connecting organic units and transition metals. Larger pore, lattice ratios, and functionalities can be obtained that make this material useful for many industrial applications.

A special group of metal organic frameworks are zeolitic imidazolate frameworks (ZIFs) with lattices that resemble simple zeolite structures [5, 6]. By varying the linkers, ligands and metals in the materials various promising applications seem possible [7]. Starting in 2006 ZIFs have been synthesized by Yaghi's group (Park et al., 2006 [8]; Hayashi et al., 2007 [9]; Wang et al., 2008 [10]) and have attracted more attention nowadays [11].

One of the key advantages of porous materials comes from the design and synthesis flexibility inherent that enables high thermal and chemical stability. Their high surface area is also of advantage. This becomes the main purpose of this study focus on the investigation of a new porous material, Zeolitic Imidazolate Framework-8 (ZIF-8) has extraordinary chemical stability in refluxing organic solvents, also in water, and aqueous alkaline solution [8, 12]. Several publications of experiments [13-18] and simulations [19-22] have been reported that guest molecules were encapsulated in ZIF-8. Conversely, the diffusion mechanisms of guest molecules and interaction parameters are still ambiguous and not established for ZIF's.

In this work, several parameter sets for the molecular interactions have been investigated to find a suitable parameter set for ZIF-8 by comparing results of molecular dynamics (MD) simulations with constant volume and energy (NVE) and with constant pressure and temperature (NPT) to the experiments. The suitable parameter set (force constants and partial charges of the ZIF-8 lattice) was employed to observe the diffusion mechanisms of guest molecules and the window size of ZIF-

8 with increasing concentration of guest molecules as studied by computational calculations such as (MD) simulations and quantum mechanics (QM) techniques.

## 1.2 Zeolitic Imidazolate Frameworks (ZIFs)

ZIFs are a new class of nanoporous compounds namely, Metal-Organic Frameworks (MOFs). ZIFs consist of tetrahedrally-coordinated metal ions (e.g. Co, Cu, Zn, etc.) linked by imidazolate or functionized imidazolate ligands (e.g. phenyl benzimidazolate and 2-methylimidazolate, etc). The angle between the metal-imidazole-metal atoms is similar to the  $145^\circ$  Si-O-Si angle in zeolites. Hence, ZIFs have zeolite-like topologies as shown in Figure 1.1.

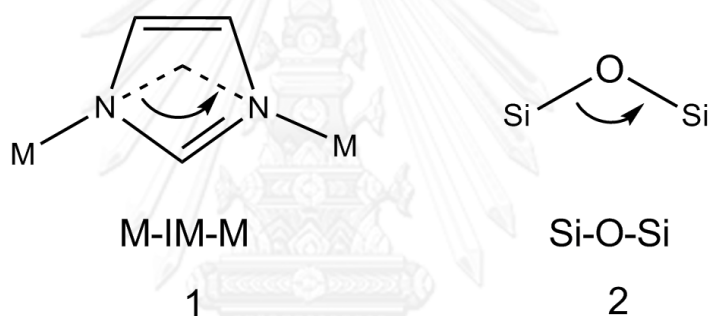


Figure 1.1 The bridging angles in ZIFs and zeolites structures: 1 is ZIF. 2 is zeolite [8].

Due to, ZIFs combine the advantages of both nanoporous materials, MOFs and zeolites: the variable pore size and chemical properties like other MOFs and the high chemical stability and the structural diversity of zeolites. Examples of ZIF topologies are shown in Figure 1.2.

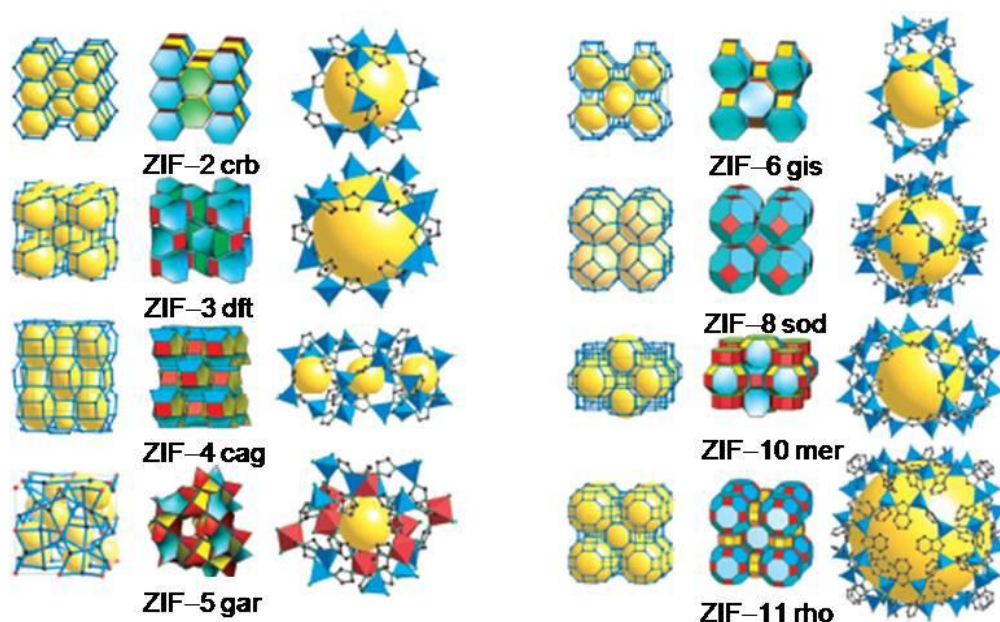


Figure 1.2 The single crystal x-ray structures of ZIFs were shown in left and center columns. The largest cage in each ZIF was shown in right column [8].

In each structure shown in Figure 1.2, the metal center is exclusively coordinated by the N atoms of the imidazolate linker. The five-membered imidazolate linker provides the bridging unit between the metal ions as shown in Figure 1.1. The organic linkers of ZIFs provide organically connected cages and channels. Therefore, ZIF structures can widely be modified to yield the desired shape, size, and surface areas by adjusting linkers and metal ions for example Zn (ZIF-1 to -4, -6 to -8, and -10 to -11) or Co (ZIF-9 and -12) with imidazolate-type links. Thus, three-dimensional porous structures with large pore volumes and high inner surface areas [8] are created.

### 1.3 Applications

Because of the diversity of ZIF topologies, the number of possible structures is huge. The concept of their design was proposed by K. S. Park and co-workers in 2006 [8]. ZIFs can be created with large surface areas up to  $1,810 \text{ m}^2/\text{g}$  and high thermal stability up to  $500 \text{ }^\circ\text{C}$ . They show remarkable efficiency for drug delivery, gas storage, catalysis, and gas separation.

### 1.3.1 Gas storage

ZIFs synthesized until now have high specific surface area. They offer plenty of space to interact with surface centers and can freely be designed to obtain various topologies by exchanging metal ion and organic linker. As a result ZIFs can absorb large amounts of light gases for industry process [8, 23].

In 2006, Park et al. [8] found that both ZIF-8 and -11 demonstrated reversible hydrogen sorption. While the hydrogen uptake of ZIF-11 at low pressure was much higher than that of ZIF-8, owing to the protruding benzene side rings of the PhIM links around which form favorable hydrogen sorption sites. However, at higher loading ZIF-8 was similar to ZIF-11 in hydrogen uptake. At about 1 atm it was 145 cm<sup>3</sup>/g at STP for ZIF-8 and 154 cm<sup>3</sup>/g STP for ZIF-11 at 77 K. The reason is that ZIF-8 has higher surface area of 1,947 m<sup>2</sup>/g and pore volume of 0.633 cm<sup>3</sup>/g than ZIF-11.

### 1.3.2 Gas separation

Like other porous materials, similar to zeolites and other MOFs, ZIFs can potentially be employed in membrane applications like separation. Hence, ZIF structures are generously designed to provide 3D pore structures with large pore size. The pore diameter can range from 2.02 to 30.1 Å [9]. They can be much larger than those of zeolites which have pore sizes of 2 to 14 Å [24]. Therefore, ZIFs have been used for gas separation [11, 13, 19, 25, 26].

Papers from Bux et al. [13] and Hertäg et al. [19] investigated the separation performance for H<sub>2</sub>/CH<sub>4</sub> mixture by experiment and diffusion of H<sub>2</sub> and CH<sub>4</sub> by simulation, respectively. Both of these works found that the diffusion of H<sub>2</sub> molecules is faster than CH<sub>4</sub>. The reason is the small size and mass of H<sub>2</sub> and its much weaker interaction with the ZIF-8 lattice. Thus, ZIF-8 is helpful for separating CH<sub>4</sub> from H<sub>2</sub>.

### 1.3.3 Catalysis

With respect to the principal units ZIFs are similar to the tetrahedral TO<sub>4</sub> of aluminosilicate zeolites and permit for construction of porous framework zeolite-like structures. Therefore, ZIFs on supporting material can be used as catalyst such as oxidation reaction [27] and Knoevenagel reaction [28] and Friedel-Crafts alkylation [29]. The interesting properties of the ZIF-based material would be interesting to the chemical industry.

ZIF-8 was also used for the Friedel-Crafts acylation reactions. Nguyen et al. [29] studied Friedel-Crafts acylation of anisole and benzoyl chloride proceeded in the presence of ZIF-8 (2-6 mol%) an inert atmosphere not necessary. The selectivity of reaction was 93%-95% to the *p*-isomer. The solid catalyst can be easily separated from the reaction mixture and can be recycled without significant loose of the catalytic activity.

### 1.3.4 Drug delivery

Previous works illustrated that the ZIF-8 had exceptional water and aqueous sodium hydroxide stability. Nevertheless, while ZIF-8 was suspended in acid solution, it initiated to decompose rapidly. Therefore, it was used to be a pH-responsive for drug carrier. Sun et al. [30] found capacity of anticancer 5-FU, loading around 660 mg of 5-FU g<sup>-1</sup> of desolvated ZIF-8. The drug released quicker from ZIF-8 in mild acidic buffer solution (pH 5.0) than at a neutral pH of 7.4. Hence, this pH-sensitivity may be used for drug delivery to tumors.

### 1.4 Zeolitic Imidazolate Framework-8 (ZIF-8)

ZIF-8 is a compound with composition Zn(MeIm)<sub>2</sub> (MeIm = 2-methylimidazolate). The structure is the SOD (sodalite) zeolite-type structure, with nanopore topology formed by 4-membered ring, 6-membered ring and ZnN<sub>4</sub> clusters as shown in Figure 1.3.

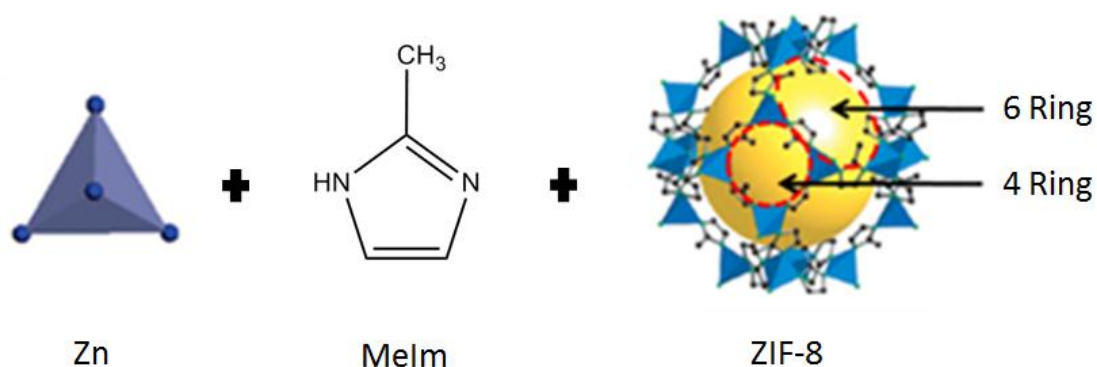


Figure 1.3 The single crystal X-ray structures of ZIF-8 that consists of Zn cluster and MeIm linker [8].

An important structural feature of the ZIF-8 framework is the existence of large pores of around 11.6 Å that are connected by apertures of 3.4 Å (6-membered ring). The aperture size of the 4-membered ring in ZIF-8 is so small that only the 6-membered ring is a real channel for moving guest molecules. In addition, the single crystal X-ray structure of ZIF-8 shows that the apparent surface area is 1,947 m<sup>2</sup>/g and the pore volume is 0.636 cm<sup>3</sup>/g [8].

### 1.5 Literature reviews

ZIF-8 has attracted interest of scientists from many fields for example experimental and simulation papers. The adsorption and diffusion of guest molecules within ZIF-8 have been variously reported. The present paper intends to study the migration of the guest molecules in this ZIF. Furthermore, the influence of the diffusing guest molecules on the lattice structure of the ZIF-8 is examined.

In 2009, Zhou et al. [31] published a paper about the hydrogen adsorption in ZIF-8 by Grand canonical Monte Carlo simulations (GCMC). They used the refined OPLSAA force field to obtain the adsorption isotherm for hydrogen in ZIF-8 at 77 K. The results are in reasonably good agreement with the experimental data. Hence, the model and the force field parameters in this work are able to reproduce the adsorption isotherm of hydrogen in ZIFs. The computer tomography for such materials advised that the first adsorption site locates at the C=C bond and the second adsorption site is within the pore channel. However, hydrogen has been adsorbed in smaller amount at the nitrogen atom that is connected with the metal center. The reason is that diameter of the hydrogen molecule is 0.23 nm, but the diameter of the free spherical spaces around the nitrogen atom and the C=C bond are 0.227 and 0.342 nm, respectively. It seems that the hydrogen molecules are adsorbed to the C=C bond easily, while hydrogen molecules cannot move easily to the free space around the nitrogen atom. In contrary, in several MOFs the preferential adsorption site is the metal center, but not on the organic linker.

In 2009, Moggach et al. [32] studied the ZIF-8 at increasing pressure of 0.18, 0.52, 0.96 and 1.47 GPa. Data and on decreasing pressure at 0.82, 0.39 and 0 GPa. Increasing the pressure, the electron density increased within the pore from 219 to 636 electron /cell. A high-pressure phase appeared that kept the symmetry of ZIF-8 but a reorientation of the imidazolate linkers was observed, increasing the size of the 6-ring windows and the pore volume. After decreasing the pressure, the structural

change was found to be reversible. Hence, larger molecules could be inserted into the pores at high pressure more easily.

In 2010, Assfour et al. [33] reported results of MD simulations of ZIF-8 and ZIF-11 loaded with molecular hydrogen. For ZIF-8, a first adsorption site with an adsorption energy of 8.6 kJ/mol is located on the top of the imidazolate ring (organic linker) over the C=C bond. The second adsorption site with adsorption energy about 6.2 kJ/mol is located at the center of the channel of the Zn hexagon (channel site). Furthermore, the H<sub>2</sub> adsorption of ZIF materials can be improved by substituting the metal in the metal cluster by B or Li. It is also suggested to exchange the organic linker could be replaced by longer organic linkers.

In 2011, Fairen-Jimenez et al. [34] examined the adsorption of N<sub>2</sub> at 77 K in two different rigid ZIF-8 structures separately (the first one ambient pressure and the other one at 1.47 GPa) in order to investigate the step in the isotherm that Moggach et al. found and to relate it to possible changes in the structure of the ZIF-8 using GCMC simulations of nitrogen at 77 K. For the ambient pressure structure, the maximum uptake corresponds to 36.9 molecules per unit cell. This is close to the first step of the experimental isotherm but, the isotherm for larger pressure is different. For simulations with the 1.47 GPa structure the maximum uptake corresponds to 49.4 molecules per unit cell, similar to the experimental data higher pressure. So, it seems that different structures must be used for different pressures. The idea of a structural transition of ZIF-8 with increasing N<sub>2</sub> loading is therefore plausible.

In 2011, Hertäg et al. [19] published the first simulations of H<sub>2</sub> and CH<sub>4</sub> in ZIF-8 by using flexible lattice. They checked AMBER and DREIDING force fields to reproduce framework flexibility of ZIF-8. For the AMBER parameter set it even turned out that lattice flexibility was the crucial factor that made diffusion of CH<sub>4</sub> molecules possible. The CH<sub>4</sub> molecules have a kinetic diameter of 3.80 Å and the window diameter of the rigid ZIF-8 lattice is 3.4 Å. By use of the flexible lattice in [8] good agreement with experimental data for this system was found and the selectivity of a ZIF-8 membrane for the H<sub>2</sub>/CH<sub>4</sub> separation measured in [13] could reproduced very well.

In 2011, Zheng et al. [35] studied a novel force field for a molecular dynamics simulation of flexible ZIF-8 and used computed partial charges and parameters derived from the AMBER. They obtained bond length, angle and box size in NPT (Isothermal-isobaric Ensemble) simulations in good agreement with experimental data. The experimental self-diffusivity for CO<sub>2</sub> was also well reproduced. The

parameters of [19] does not reproduce the box size in NPT. However, the parameter set [19] is more successful with respect to diffusion property such as  $H_2$  and  $CH_4$  molecules in NVE (Microcanonical Ensemble simulations) because the window size is most important which is better reproduced in [19]. The cell size is an input parameter and constant and therefore, exact by definition in NVE.

In 2013, Zhang et al. [36] use a self-developed parameter set for hybrid simulation methods between Monte Carlo and MD simulations that can describe the structural change in the ZIF-8 lattice induced by the guest molecules, a phenomenon which is usually named gate opening. This effect was for the first time reproduced in MD simulations. The results from adsorption isotherms lead to the assumption that guest molecules induced structural changes of the lattice happening at higher loadings with  $N_2$  molecules. The structural transition of ZIF-8 from the low-loading to high-loading structure was found as well as the reorientation of the imidazolate linker. Furthermore, the radial distribution functions between  $N_2$  and the framework atoms indicate strong attraction between  $N_2$  and the imidazolate rings.

Numerous experimental methods have been applied to understand the adsorption and diffusion of guest molecules inside ZIF-8. Experimental data provide a powerful and straightforward route to get knowledge. Theoretical calculation methods form another powerful tool to investigate the behavior of guest molecules in ZIF-8 in microscopic detail and conclusions drawn from simulations yield valuable guidelines for improvement of new ZIFs.

The main purpose of this research is to study several parameter sets for the molecular interactions of ZIF-8 and to investigate the adsorption and diffusion of guest molecules in molecular detail. With the chosen set of parameters not only diffusion but, also the effect of the diffusing molecules on the window size has been investigated by MD simulations.

## 1.6 Scope of this study

This study includes a part dealing with force field parameters for the molecular interactions of ZIF-8 by comparing results of MD simulations with experiments. The obtained suitable parameter set was used to investigate the self-diffusion coefficient and the windows size as functions of the concentration of ethane and nitrogen guest molecules in the flexible ZIF-8 framework. These guest molecules can be found gate-opening effect in ZIF-7 and ZIF-8.



Moreover, the rotational energies of organic linkers of ZIF-8 structure located at the windows for 4- and 6-membered rings were examined by quantum chemical calculations. That is related to the gate-opening phenomena.



## CHAPTER II

### THEORY BACKGROUND

The molecular modeling technique is a powerful and modern tool for solving scientific problems as numerical experiments can be performed for new materials without synthesizing them. This has been confirmed by the Nobel Prize in Chemistry in 2013 to a Molecular Simulation team. Aims of this technique are to reproduce experiments to elucidate the invisible microscopic details and moreover to explain experiments. Conversely, simulation can also be used as a useful predictive instrument [37]. This is the case when dealing with processes and properties of gas adsorption systems in porous material, in the present case ZIF-8.

In general, molecular modeling proceeds in three stages. First stage a model is chosen to describe the intra- and inter-molecular interactions in the system by using several common methods. These are quantum mechanics, molecular mechanics and fitting to experimental data (different from quantities under investigation). With these methods the energy of configurations of the atoms and molecules in the system can be calculated. This allows to determine how the energy of the system varies with the positions of the atoms and molecules. Then Molecular Dynamics or Monte Carlo simulations are carried out. The result of the simulation is a time series of conformations; called a trajectory. Finally, the calculation must be analyzed, to calculate properties and to check that the simulations have been performed properly [38].

#### 2.1 Molecular dynamics simulations

According to [39, 40], Molecular Dynamics (MD) simulations compute the trajectory of individual molecules in the systems. The basic idea here is motion, which describes how positions, velocities, and orientations vary with time. In effect, molecular dynamics constitutes a motion picture that follows molecules as twisting, turning, colliding with one another, and, perhaps, colliding with their container. In a classical MD simulation, the trajectory is calculated by integrating Newton's equations of motion. The integration must be done numerically using one of some well known numerical integrators and the potential energy function.

### 2.1.1 Classical mechanics

The MD simulation method is supported from Newton's second law or another equation of motion with boundary conditions appropriate for the geometry or symmetry of the system. Knowledge of the force on each atom and of configurational energy is needed. Integration of the equations of Newton's second law then yields a trajectory which yields the development positions, velocities and accelerations of the atoms with time. Using this trajectory, the average values of properties can be estimated. The positions and velocities of each atom in the system can be calculated at any time in the future or the past.

Newton's equation of motion is given by equation (2.1) when  $\vec{F}_i$  is the total force of atom  $i$ ,  $m_i$  is the mass of atom  $i$  and  $\vec{a}_i$  is the acceleration of atom  $i$ .

$$\vec{F}_i = m_i \vec{a}_i \quad (2.1)$$

Then, the force can be calculated it from the gradient of the potential energy by equation (2.2). Afterward, combining these two equations yields from (2.1) and (2.2) are giving in equation (2.3) when  $U$  is the potential or configurational energy of the system. Therefore, Newton's equations of motion related with the potential energy for changing the position as a function of time are:

$$\vec{F}_i = -\nabla_i U \quad (2.2)$$

$$\vec{F}_i = -\frac{\partial U}{\partial \vec{r}_i} = m_i \frac{\partial^2 \vec{r}_i}{\partial t^2} = m_i \vec{a}_i \quad (2.3)$$

For a unique solution the knowledge of the initial positions and velocities of the atoms is necessary. Thus, positions and velocities at any time are determined by the initial positions and velocities.

The average positions of the lattice atoms can be obtained from experimental structures such as the X-ray crystal structure determined by NMR spectroscopy. These can be used as initial position of the lattice atoms while the initial positions of the guests are chosen randomly.

The initial velocities ( $\vec{v}_{i0}$ ) are usually selected randomly from a Maxwell-Boltzmann or Gaussian distribution at a given temperature, which gives the

probability density ( $W$ ) that an atom  $i$  has a velocity  $v_x$  in the  $x$  direction at a temperature ( $T$ ) shown in equation (2.4).

$$W(\vec{v}_{ix}) = \left( \frac{m_i}{2\pi k_B T} \right)^{1/2} \exp \left( -\frac{1}{2} \frac{m_i \vec{v}_{ix}^2}{k_B T} \right) \quad (2.4)$$

The velocities are corrected to fulfill.

$$\vec{P} = \sum_{i=1}^N m_i \vec{v}_i = 0 \quad (2.5)$$

The temperature can be estimated from the velocities using equation (2.6) when  $N$  is the number of atoms in the system using the equipartition theorem of statistical mechanics.  $k_B$  is Boltzmann constant.

$$T = \frac{1}{(3Nk_B)} \sum_{i=1}^N \frac{|\vec{P}_i \cdot \vec{v}_i|}{m_i} \quad (2.6)$$

During the MD simulation the sites and velocities are stored. The trajectory can be used to evaluate configurational properties (positions, velocities and accelerations) and dynamic quantities like transport coefficients and time correlation functions of all  $N$  particles from the trajectory [41, 42].

### 2.1.2 Integration algorithms

For given initial conditions and potential energy functions, a finite difference approximation is used to calculate numerically the trajectory of all  $N$  particles in the system. Many numerical algorithms are proposed to carry out the integration processes in molecular dynamics for integrating the equations of motion such as the Leapfrog, the Verlet, the Toxvaerd and the Gear algorithm. The algorithm should conserve energy and momentum, it should be computationally efficient. For the simulations of this work, the Velocity-Verlet algorithm has been chosen which is the most common one.

This algorithm determines positions, velocities and accelerations and combines two Taylor expansions, as follows. The Taylor series for position from time  $t$  forward to  $t + \Delta t$  is:

$$\vec{x}_i(t + \Delta t) = \vec{x}_i(t) + \frac{d\vec{x}_i(t)}{dt} \Delta t + \frac{1}{2} \frac{d^2\vec{x}_i(t)}{dt^2} \Delta t^2 + \frac{1}{3!} \frac{d^3\vec{x}_i(t)}{dt^3} \Delta t^3 + O(\Delta t^4) \quad (2.7)$$

The Taylor series from  $t$  backward to  $t - \Delta t$  is:

$$\vec{x}_i(t - \Delta t) = \vec{x}_i(t) - \frac{d\vec{x}_i(t)}{dt} \Delta t + \frac{1}{2} \frac{d^2\vec{x}_i(t)}{dt^2} \Delta t^2 - \frac{1}{3!} \frac{d^3\vec{x}_i(t)}{dt^3} \Delta t^3 + O(\Delta t^4) \quad (2.8)$$

Adding these two expansions eliminates all odd-order terms, leaving

$$\vec{x}_i(t + \Delta t) = 2\vec{x}_i(t) - \vec{x}_i(t - \Delta t) + \frac{d^2\vec{x}_i(t)}{dt^2} \Delta t^2 + O(\Delta t^4) \quad (2.9)$$

This is Verlet's algorithm for the positions. It has a local truncation error that varies as  $(\Delta t^4)$  and hence is fourth order, even though it contains no third-order derivatives. Nor does (2.9) for positions involve any function of the velocities. The acceleration in (2.9) is, of course, obtained from the intermolecular forces. To estimate velocities, practitioners have contrived various schemes, one being an estimate for the velocity at the half-step:

$$\vec{v}_i \left( t + \frac{1}{2} \Delta t \right) \approx \frac{\vec{x}_i(t + \Delta t) - \vec{x}_i(t)}{\Delta t} \quad (2.10)$$

Verlet himself used the first-order central difference estimator.

$$\vec{v}_i(t) \approx \frac{\vec{x}_i(t + \Delta t) - \vec{x}_i(t - \Delta t)}{2\Delta t} \quad (2.11)$$

Verlet's algorithm is a two-step method because it estimates  $\vec{x}_i(t + \Delta t)$  from the current position  $\vec{x}_i(t)$  and the previous position  $\vec{x}_i(t - \Delta t)$ . Therefore it is not self-

starting: initial positions ( $\vec{x}_0$ ) and velocities ( $\vec{v}_0$ ) are not sufficient to begin a calculation, and something special must be done for example assumptions about  $x(-\Delta t)$  can be made. The Verlet algorithm is simple and has very good stability for moderately large time steps. In its original form molecular velocities do not appear, in conflict with the attitude that the phase-space trajectory depends equally on positions and velocities. Modern formulations [43, 44] of the method often overcome this asymmetric view.

### 2.1.3 Force field

The force field and the potential energy function refer to the interaction between the atoms and depend only on the configuration *i.e.* the positions. The forces acting on atoms and move them into new position consist of two components such as intramolecular or bonded and intermolecular or non-bonded potentials. The potential function involves the sum over these terms.

$$U_{total} = \sum U_{bonded} + \sum U_{non-bonded} \quad (2.12)$$

#### 2.1.3.1 Intramolecular potential

The intramolecular potential or bonded potential ( $U_{bonded}$ ) is describing chemical bonds such as bond-stretching, angle-bending, and torsion potentials. The energy  $U_{bonded}$  is calculated as a sum of  $U_{bond}$ ,  $U_{angle}$  and  $U_{torsion}$  [38, 45].

$$U_{bonded} = U_{bond} + U_{angle} + U_{torsion} \quad (2.13)$$

Which corresponds to three types of atom geometry as show in Figure 2.1.

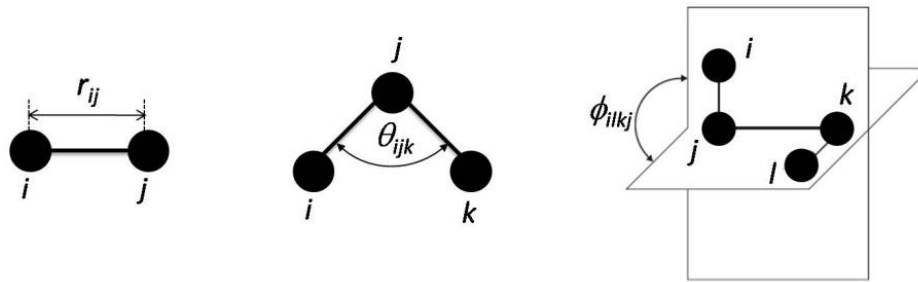


Figure 2.1 The bonded potential; (a) The bond-stretching potential. (b) The angle bending potential. (c) The torsional potential (also called dihedral potential).

The first term bond-stretching potential energy ( $U_{bond}$ ) in the equation (2.13) contains the energy function for stretching a bond between two atom types  $i$  and  $j$  by using an harmonic potential. The configurational energy of a bond is a function of the deviation of the bond length from the “equilibrium” value ( $r_0$ ). The force constant ( $k_r$ ) indicates the strength of the bond. The equilibrium bond lengths and the force constants are defined for each pair of bonded atoms and both of them rely on the chemical type of atom components as written as equation (2.14).

$$U_{bond} = \sum_{bonds} k_r (r_{ij} - r_0)^2 \quad (2.14)$$

When  $r_{ij}$  being the absolute value of  $\vec{r}_{ij} = \vec{r}_i - \vec{r}_j$ .

The second term in (2.13) refers to the angle-bending potential energy ( $U_{angle}$ ) equation is the energy required for bending an angle formed by three atoms ( $i-j-k$ ), where there is a bond between  $i$  and  $j$ , and between  $j$  and  $k$ . This is also an harmonic potential.  $\theta_0$  and  $k_r$  rely on the chemical types of atoms forming the angle. This leads to the following equation (2.15).

$$U_{angle} = \sum_{angles} k_\theta (\theta_{ijk} - \theta_0)^2 \quad (2.15)$$

The final term, the torsion potential energy ( $U_{torsion}$ ) in the equation (2.13) describes the part of the energy change associated with rotation in a four-atom sequence  $i-j-k-l$ , where  $i-j$ ,  $j-k$  and  $k-l$  are bonded. The rotational motion related with this term is described by a dihedral angle and a coefficient of symmetry

$m$  (periodicity), around the central bond  $j-k$ . This potential is supposed to be periodic and is regularly demonstrated by a cosine function as given in equation (2.16).

$$U_{\text{torion}} = \sum_{\text{torsions}} k_{\phi} [1 + \cos(m\phi_{jkl} - \phi_0)] \quad (2.16)$$

The values of force constant ( $k_{\phi}$ ) can be obtained from experimental data (such as infrared spectral frequencies) or from quantum mechanical calculations.

### 2.1.3.2 Intermolecular potential

Intermolecular potentials or non-bonded potentials ( $U_{\text{non-bonded}}$ ) [37, 46] involve electrostatic or Coulomb and Van Der Waals potentials. A typical expression for such a potential is:

$$U_{\text{non-bonded}} = U_{\text{Van Der Waals}} + U_{\text{electrostatic}} \quad (2.17)$$

The first term in equation (2.17) is the Van Der Waals interaction between two atoms ( $U_{\text{Van Der Waals}}$ ) that results from a sum of repulsive and attractive forces as presented in Figure 2.2, using a simple empirical term that can be easily calculated. The potential function should to be rapidly calculated because of the large number of Van Der Waals interactions that must be calculated during one simulation.

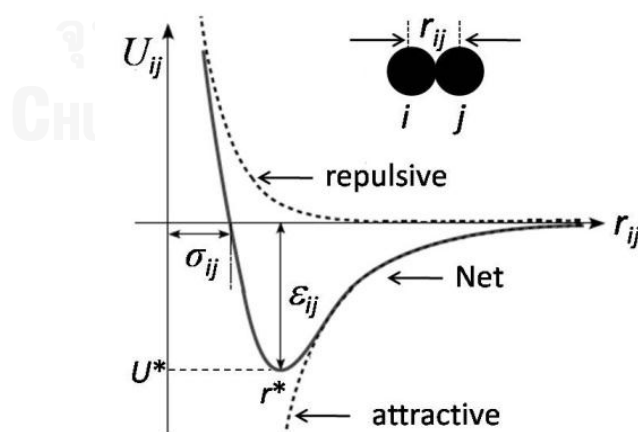


Figure 2.2 Van Der Waals interaction between two atoms including repulsive and attractive forces.



The most popular Van Der Waals potential function is the Lennard-Jones function. The interaction between two atoms is given by this function as:

$$U_{Van\ Der\ Waals} = \sum_{i < j} 4\epsilon_{ij} \left[ \left( \frac{\sigma_{ij}}{r_{ij}} \right)^{12} - \left( \frac{\sigma_{ij}}{r_{ij}} \right)^6 \right] \quad (2.18)$$

When  $\sigma_{ij}$  is the value of the minimum depth of the potential energy for the interaction involving atom  $i$  and  $j$ ,  $\sigma_{ij}$  (the separation distance for which the energy is zero) and  $r_{ij}$  shows the distance between the atom centers.

Normally, both  $\sigma_{ij}$  and  $\epsilon_{ij}$  parameters depend upon both atom types. There are many ways of combining atomic parameters of pure substances to parameters for mixtures, some of them quite complicated. In this study, Lorentz–Berthelot mixing rules are used, which are:

$$\sigma_{ij} = \frac{1}{2}(\sigma_{ii} + \sigma_{jj}) \quad (2.19)$$

and

$$\epsilon_{ij} = \sqrt{\epsilon_{ii} \epsilon_{jj}} \quad (2.20)$$

Where  $\sigma_{ii}$ ,  $\sigma_{jj}$ ,  $\epsilon_{ii}$  and  $\epsilon_{jj}$  are the LJ diameters for the interaction of  $i$ - $i$  atoms and so on.

The second term in equation (2.17) is the electrostatic interaction ( $U_{electrostatic}$ ) between a pair of atoms for example attractive potential as see in Figure 2.3.

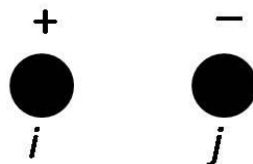


Figure 2.3 Electrostatic interaction between a pair of atoms.

The fundamental equation of electrostatics is Coulomb's law as shown in equation (2.21), which describes the force between two point charges.  $\epsilon_0$  is the effective dielectric function for the medium and  $r_{ij}$  is the distance between two atoms having charges  $q_i$  and  $q_j$ .

$$U_{Coulomb} = \sum_{i < j} \frac{1}{4\pi\epsilon_0} \frac{q_i q_j}{r_{ij}} \quad (2.21)$$

The derivations of the potential energy function with respect to the atomic coordinates yield the forces needed in a molecular dynamics simulation.

#### 2.1.4 Periodic Boundary Conditions

Molecular dynamics is typically applied to systems containing several hundred or a few thousand atoms. To avoid surface effects for particles close to the wall of the simulation box, periodic boundary conditions are used. Imagine a cubic box containing particles which is replicated in all directions to form a periodic array. In the two-dimensional example shown in Figure 2.4. Each box is surrounded by eight neighbors. For three dimensions each box would have 26 nearest neighbors. The coordinates of the particles in the image boxes can be obtained by adding or subtracting integral multiples of the box edge length. Should a particle leave the box then an image particle enters from the opposite side simultaneously, as shown in Figure. 2.4. Thus the number of particles within the central box remains constant.

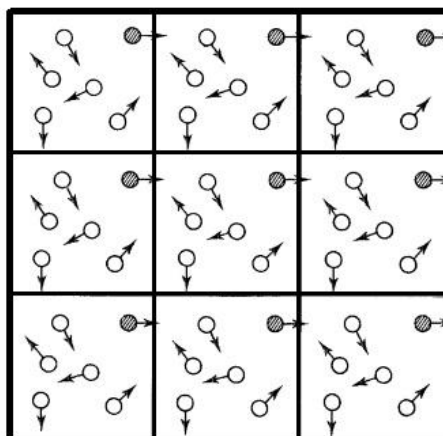


Figure 2.4 Electrostatic interaction between a pair of atoms.

The cubic cell is the simplest periodic system to visualize and to program. However, a cell of a different shape might be more appropriate for a given simulation. This may be particularly important for simulations of systems which comprise a single molecule or intermolecular complex surrounded by solvent molecules. In such systems it is usually the behavior of the central solute molecule that is of most interest and so it is desirable that as little of the computer time as possible is spent simulating the solvent far from the solute.

For some simulations it is inappropriate to use standard periodic boundary conditions in all directions. For example, when studying the adsorption of molecules onto a surface, it is clearly inappropriate to use the usual periodic boundary conditions in direction to the surface. Rather, the surface is modeled as a true boundary, for example by explicitly including the atoms in the surface or considering the surface to be a wall. In case of a hard wall each arriving particle is reflected back into the simulation cell. The opposite side of the box must be treated in a similar way [37, 39].

### 2.1.5 Ensembles

In this part, MD was for the “typical” MD ensemble, which holds particle number, system volume, and total energy constant (NVE). Additionally in the common NVE-MD also the total momentum is conserved. There are three important ensembles in the theory of statistical thermodynamics, and they are classified according to what is kept constant in each system as following [47].

- Microcanonical ensemble (NVE): The thermodynamic state is determined by a fixed number of atoms ( $N$ ), a fixed volume ( $V$ ), and a fixed energy ( $E$ ). This corresponds to an isolated system.
- Canonical Ensemble (NVT): This ensemble describes a system in contact with a heat bath. Its thermodynamic state is defined by a fixed number of atoms ( $N$ ), a fixed volume ( $V$ ), and a fixed temperature ( $T$ ). Energy can be exchanged with the bath that has the wished temperature.
- Isobaric-Isothermal Ensemble (NPT): This ensemble is characterized by the number of atoms ( $N$ ), the pressure ( $P$ ), and the temperature ( $T$ ). Energy can be exchanged with the heat bath and volume can be exchanged with the “pressure” bath.

### 2.1.6 Principle of diffusion

Diffusion is the transport process of nature where atoms or molecules migrate by irregular thermal motion.

Two categories of diffusion can be found such as transport diffusion caused by a concentration gradient, which generates a particle stream from the region of high concentration to one of low concentration and self-diffusion, which is a mixing migration by irregular thermal motion [48, 49].

#### 2.1.6.1 Transport diffusion

The backgrounds of the hypothesis of diffusion were revealed by Fick in the 19th century. The particle flow can be connected to the concentration gradient according to Fick's first law [50]. In one dimension it reads:

$$J = -D_t \left( \frac{\partial C}{\partial x} \right) \quad (2.22)$$

$C$  is the concentration.  $x$  is the position, and  $D_t$  is the transport diffusion coefficient.

The diffusion coefficient is identified as a constant between the rate of flow and the concentration gradient. While the above equation is the starting point for the treatment of transport diffusion, it does not explain the driving force of diffusion. The driving force for transport diffusion is the gradient of the chemical potential  $\mu$ . By irreversible thermodynamics, the Onsager reciprocal relations ( $L$  is the Onsager coefficient) can be derived yielding equation (2.23).

$$J = -L \left( \frac{\partial \mu}{\partial x} \right) \quad (2.23)$$

This equation categorizes the basis for transport diffusion. The work on porous material diffusion of Barrer and Jost [51] was based on Fick's equation. Assuming a concentration-independent diffusion constant, from equation (2.22) Fick's second law can be derived.

$$\frac{\partial C}{\partial t} = D_t \left( \frac{\partial^2 C}{\partial x^2} \right) \quad (2.24)$$

Equation (2.24) provides the change of concentration in time and space. In the approach of Barrer and Jost, the diffusivity is assumed to be isotropic, as  $D_t$  is independent of the direction in which the particles diffuse. In this macroscopic equation all information about the exact shape and connectivity of the pore structure is missing. It contains only a global value of the diffusion constant [49].

### 2.1.6.2 Self-diffusion

This kind of diffusion can be observed by labeling some of the molecules and following the motion of labeled and unlabeled molecules. Equation (2.22) can be applied to depict the flow of the labeled particles in equation (2.25).  $J_i^*$  is flux density of labeled particle and  $C^*$  is the number density of labeled particle, and  $D_s$  in this equation is the self-diffusion constant.

$$J_i^* = -D_s \left. \frac{\partial C^*}{\partial x_i} \right|_{C=\text{constant}} \quad (2.25)$$

Otherwise, the self-diffusion constant can be referred to a microscopic property identified by the mean-square displacement, as it was demonstrated by Einstein in his study on Brownian motion [52]. The mean-square displacement is described in equation (2.26).  $N$  refers to the number of particles in the system and  $\vec{r}^j(t)$  show the position of molecule  $j$  at time  $(t)$  that is the average of the squared distance that a molecule has moved at time  $(t)$ .

$$\langle r^2(t) \rangle = \langle |\vec{r}(t) - \vec{r}(0)|^2 \rangle = \frac{1}{N} \sum_{j=1}^N (\vec{r}^j(t) - \vec{r}^j(0))^2 \quad (2.26)$$

In supposing that the molecules move by a random walk thus it can be explained that for suitably extended times the mean-square displacement will be linearly dependent on time [53].

$$\left\langle \left| \vec{r}^2(t) \right| \right\rangle = 6D_s t \quad (2.27)$$

This equation is the well-known Einstein relation. It can be revealed that the diffusion constant in equation (2.25) and (2.27) are not different [54]. Another method to derive the self-diffusivity from microscopic properties of the diffusing molecules is by conception of the Green-Kubo relations [55]. With this relation, the self-diffusivity can be obtained from the velocity auto-correlation function, a property that describes correlations involving velocities at different times as shown in equation (2.28).

$$D_s = \frac{1}{3} \int_0^{\infty} \left\langle \vec{v}(0) \cdot \vec{v}(t) \right\rangle dt \quad (2.28)$$

Even though, it is complicated to evaluate the velocity auto-correlation function in the experiment, this equation can be easily applied in theoretical techniques like MD simulation [49].

### 2.1.7 Radial distribution function

The radial distribution function (RDF) usually named  $g(r)$ , or pair correlation function is the probability of finding an atom at a distance of  $r$  away from a given reference atom. Specifically, it is proportional to the probability of finding two atoms with distance in  $r \pm \Delta r$  as shown in Figure 2.5. The mathematical definition of  $g(r)$  [39] is given as following in equation (2.29).

$$ng(r) = \frac{1}{N} \left\langle \sum_i^N \sum_{j \neq i}^N \delta[r - r_{ij}] \right\rangle \quad (2.29)$$

Here  $N$  is the total number of atoms,  $n = N/V$  is the number density,  $r_{ij}$  is the distance between centers of atoms  $i$  and  $j$ , the angular brackets mean a time average and  $\delta(x)$  is the delta function.

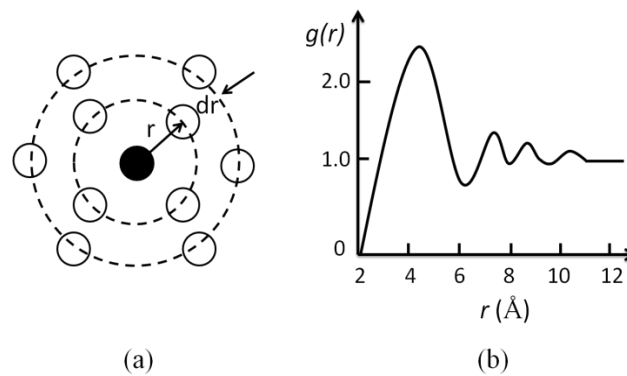


Figure 2.5 (a) Graphic of the particles in a simple atomic liquid and (b) schematic example of a radial distribution function as it could result from a simulation.

The RDF plays a central role in statistical mechanical theories of dense gases and fluids and for adsorption at surfaces and in pores. Since molecular dynamics yields positions of all individual atoms as a functions of time,  $g(r)$  can be readily computed from molecular dynamics trajectories as shown in Figure 2.5 (b). At short distances (less than the atomic diameter)  $g(r)$  must be zero. Because of the strong repulsive forces particles cannot approach close to each other. The first peak, indicates the probability that two particles are found in contact. The radial distribution function then becomes smaller and has a minimum. The chances of finding two atoms with this separation are less than finding them in contact. At long distances,  $g(r)$  approaches to one indicating that there is no long-rang order. The pair distribution function is calculated from a simulation by sorting the neighbors around each atom into distance bins. The number of neighbors in each bin is averaged over the entire simulation. This calculation can be done during the simulation or by analyzing the stored trajectory. Equation (2.30) is used to evaluate the radial distribution function.

$$g(r, \Delta r) = \frac{V}{N^2} \frac{\langle N(r, \Delta r) \rangle}{4\pi r^2 \Delta r} \quad (2.30)$$

$N(r, \Delta r)$  is the number of atoms found in the bin of radius  $r$  and thickness  $\Delta r$ ,  $4\pi r^2 \Delta r$  is the volume of a spherical shell with thickness  $\Delta r$ .

Also, this expression can be physically interpreted as the ratio of a local density  $n(r)$  to the system density  $n$ , as written in equation (2.31).

$$g(r) = \frac{n(r)}{n} \quad (2.31)$$

Experimentally radial distribution functions can be obtained from x-ray and neutron diffraction experiments. The X-ray diffraction pattern can be used to calculate an distribution function from experiment, which can then be compared with that obtained from the simulation [37, 45].

## 2.2 Quantum chemistry

All quantum chemical models are derived from the Schrödinger equation published in the late 1920's. It describes molecules as being composed of nuclei and electrons. The solution of the Schrödinger equation describes the motions of electrons, which in turn leads directly to molecular structure and energy among other observables and also provides information about bonding [56]. For instance, we can calculate molecular energies, molecular structures geometry optimizations and potential energy surfaces for 4-membered and 6-membered rings of ZIF-8.

Structures of molecules can be described by the time independent Schrödinger equation.

### 2.2.1 The Schrödinger equation

The molecular geometry can be found in terms of minimum energy arrangements of nuclei [57]. Every description of quantum mechanical systems finally is based on the Schrödinger equation, which only for the unique case of an hydrogen atom (a single non-relativistic particle) may be solved exactly. The time independent version of the Schrödinger equation reads.

$$E\psi(q) = \frac{-\hbar^2}{2m} \nabla^2 \psi(q) + U(q)\psi(q) \quad (2.32)$$



When  $m$  is the particle of mass,  $U$  is potential energy,  $\nabla^2$  is Laplacian,  $E$  is the electronic energy in atomic units,  $\Psi$  is a function of the electron coordinates and  $q$  describes the motion of the electron as fully as possible. Wavefunctions ( $\Psi$ ) for the hydrogen atom are described by the atomic orbitals.

The square of the wavefunction times a small volume gives the probability of finding the electron in this volume. Hence,  $\Psi\Psi^*$  is termed the total electron density (or more simply the electron density), and corresponds to the electron density evaluated in an X-ray diffraction experiment. It is easy to simplify the Schrödinger equation to a multinuclear, multielectron system.

$$\hat{H}\Psi = E\Psi \quad (2.33)$$

In this system,  $\Psi$  is a many-electron wavefunction and  $\hat{H}$  is the Hamiltonian operator which in atomic units is given by equation (2.34).

$$\hat{H} = -\frac{1}{2} \sum_i^{\text{electrons}} \nabla_i^2 - \frac{1}{2} \sum_A^{\text{nuclei}} \frac{1}{M_A} \nabla_A^2 - \sum_i^{\text{electron}} \sum_A^{\text{nuclei}} \frac{Z_A}{r_{iA}} + \sum_{i<j}^{\text{electron}} \sum_{ij} \frac{1}{r_{ij}} + \sum_{A<B}^{\text{nuclei}} \sum \frac{Z_A Z_B}{R_{AB}} \quad (2.34)$$

$Z$  is the nuclear charge,  $M_A$  is the proportion of mass of nucleus  $A$  to the mass of an electron,  $R_{AB}$  is the distance between nuclei  $A$  and  $B$ ,  $r_{ij}$  is the distance between electrons  $i$  and  $j$  and  $r_{ij}$  is the distance between electron  $i$  and nucleus  $A$ .

The many-electron Schrödinger equation cannot be solved exactly even for a straightforward two-electron system for example helium atom molecule. Approximations need to be established to afford practical methods [56, 58, 59].

### 2.2.2 Born-Oppenheimer approximation

One method to solve the Schrödinger equation for molecular systems approximately is to suppose that the nuclei should not move. Naturally, nuclei should move, but their movement is not fast compared to the speed of moving electrons. This is called the Born-Oppenheimer approximation. It leads to the “electronic” Schrödinger equation.

$$\hat{H}^{\text{el}} \Psi^{\text{el}} = E^{\text{el}} \Psi^{\text{el}} \quad (2.35)$$

$$\hat{H}^{\text{el}} = -\frac{1}{2} \sum_i^{\text{electrons}} \nabla_i^2 - \sum_i^{\text{electrons}} \sum_A^{\text{nuclei}} \frac{Z_A}{r_{iA}} + \sum_{i < j}^{\text{electrons}} \sum \frac{1}{r_{ij}} \quad (2.36)$$

In equation 2.34 the nuclear kinetic energy is set equal to zero to yield equation (2.36), and the nuclear-nuclear Coulomb term in equation (2.36) is a constant that must be added to the electronic energy ( $E^{\text{el}}$ ), to yield the total energy ( $E$ ) for the system.

$$E = E^{\text{el}} + \sum_{A < B}^{\text{nuclei}} \sum \frac{Z_A Z_B}{R_{AB}} \quad (2.37)$$

The nuclear mass disappears in the electronic Schrödinger equation. If the Born-Oppenheimer approximation is valid then the calculation of molecular structure and relative energetics among other important “chemical observables” becomes possible with the electronic Schrödinger equation [56, 60].

### 2.2.3 Hartree-Fock approximation

The electronic Schrödinger equation is still too complicated and to be solved needs approximations. The easiest understandable is to assume that electrons move separately of each other. In general, each of the electrons is described by a function termed molecular orbital, each of which is resolved by assuming that the electron is moving inside an average field of all the other electrons. The total wavefunction is written in the type of a single determinant (Slater determinant). The set of molecular orbitals leading to the lowest energy are achieved by a procedure referred to as a self-consistent-field (SCF process). The typical SCF procedure is the Hartree-Fock process, although SCF methods as well contain density functional process. All SCF procedures lead to equations (2.38).

$$f(i) \chi(x_i) = \epsilon \chi(x_i) \quad (2.38)$$

At this point, the Fock operator  $f(i)$  can be printed.

$$f(i) = -\frac{1}{2} \nabla_i^2 + v^{\text{eff}}(i) \quad (2.39)$$

$X_i$  show spin and coordinates of the electron  $i$ ,  $\chi$  explains the spin orbitals and  $v^{\text{eff}}$  is the effective potential of the electron  $i$ , which relies on the spin orbitals of the other electrons.

The useful potential  $v^{\text{eff}}$  depends on the SCF process [56, 61, 62].

### 2.2.4 LCAO approximation

The Hartree-Fock approximation leads to a set of paired differential Hartree-Fock equations, each relating the coordinates of a single electron. It is helpful to initiate a further approximation in order to convert the Hartree-Fock equations into a set of algebraic equations. It is logical to assume that the one-electron solutions for many electron molecules will be similar to the solutions for the hydrogen atom. Molecules consist of atoms. In general, the molecular orbitals are linear combinations of a basis set well-known by basis functions ( $\phi$ ).

$$\psi_i = \sum_{\mu} c_{\mu i} \phi_{\mu} \quad (2.40)$$

$c_{\mu i}$  are the unknown molecular orbital coefficients, frequently referred to as the molecular orbitals. Since the  $\phi$  are usually centered at the nuclear positions, they are referred to as atomic orbitals. In equation (2.40) is termed the linear combination of atomic orbitals or LCAO approximation [56].

### 2.2.5 Density functional theory

The electron correlations can e.g. be described by density functional theory (DFT). Density functional models have the electron density in contrast to the many-electron wavefunction. There are some agreements and some differences between traditional wavefunction-based approaches and electron-density-based methods. First, the necessary construction blocks of a many-electron wavefunction are single-electron orbitals, that are straightly analogous to the orbitals employed in density

functional methods. Next, both the electron density and the many electron wavefunction are assembled from an SCF approach which involves identical matrix elements [56].

The DFT of Kohn and Sham [63] is the sum of the exchange and correlation energies of a uniform electron gas. In the Kohn-Sham formalism, the ground-state electronic energy is written as a sum of the kinetic energy, the electronuclear interaction energy, the Coulomb energy and the exchange/correlation energy. Three types of exchange/correlation functionals are presently in use: *(i)* functionals based on the local spin density approximation, *(ii)* functionals based on the generalized gradient approximation, and *(iii)* functionals which use the exact Hartree-Fock exchange [56, 63].

The DFT is an exact theory and the only approximation is due to that exchange correlation energy is unknown. The basis sets for these Kohn Sham (KS) orbitals have fewer requirements than those in Hartree-Fock. They are not needed for calculating exchange and Coulomb interaction which are the most work consuming part of the Hartree-Fock method. This, and the fact that DFT account for electron correlation, make DFT very useful for larger systems. However, the crucial task in DFT is to find an accurate exchange correlation functional. The most popular exchange-correlation functional is the B3LYP functional. It includes numerous functionals, with the Hartree-Fock exact exchange energy in a three-parametric system [64, 65].

### 2.2.6 Basis set

The set of statistical functions that creates the molecular orbital (MO) in the linear combination of atomic orbitals (LCAO) is called a basis set, which is developed as a linear combination of such functions with coefficients to be determined. Generally these functions are atomic orbitals, in that they are centered on atoms, but functions centered in bonds or lone pairs, and pairs of functions centered in the two lobes of a p orbital, have been employed. Furthermore, basis sets invent from sets of plane waves down to a cutoff wavelength are regularly applied, principally in calculations relating systems with periodic boundary conditions [45, 62].

### 2.2.6.1 Effective core potential

Effective core potential (ECP) basis sets have been employed in this work for performing valence only computations containing transition-metal atoms with accuracies approaching all-electron calculations at a portion of the computational cost such as LANL2DZ. The latter is of double zeta (DZ) quality and the overall grouping of ECP and valence basis set is thus referred to LANL2DZ basis. The method utilized here for generation of ECP's follows the basic method expressed by Kahn, Baybutt, and Truhlcu [66] for the nonrelativistic case and by Kahn, Cowan, and Hayll for the relativistic case. The sequence of steps is outlined below and each step is described in greater detail in the following sections [67].

- The "core" orbitals to be replaced and the remaining "valence" orbitals are described.
- Numerical valence orbitals are get from self-consistent (nonrelativistic or relativistic) and Hartree-Fock calculations is one order of magnitude larger than the highest angular momentum quantum number of any core orbital.
- Smooth, nodeless pseudo-orbitals are obtained from the Hartree-Fock orbitals in a manner so that perform as closely as possible to in the outer, valence region of the atom.
- Numerical effective core potentials are gained by demanding that is a solution in the field with the same orbital energy as the orbital.
- The numerical potentials fitting in analytic form with Gaussian functions.
- The numerical pseudo-orbitals are also fit with Gaussian functions to achieve basis sets for molecular calculations.

## CHAPTER III

### CALCULATION DETAILS

#### 3.1 Molecular dynamics (MD) simulations

It is not easy to find force fields that can describe property the lattice flexibility of ZIFs. Hertäg et al. [19] used the slightly modified AMBER force field. They were successful to describe the separation of H<sub>2</sub> and CH<sub>4</sub> by a ZIF-8 membrane. This model could also describe well the ZIF-8 lattice structure, particularly the size and shape of the windows. These MD simulations were done in the NVE ensemble. In this ensemble the simulation box size is constant and therefore agrees with X-ray data.

Alternatively, the MD simulations can be carried out in the NPT ensemble although the pressure inside porous solids is an ambiguous quantity. In this case the box size can vary and the model of [19] leads to a somewhat smaller average unit cell size.

Zheng et al. [35] and Zhang et al. [36] proposed other force fields to perform MD simulations. In their simulations in the NPT ensemble the unit cell size of the flexible ZIF-8 was reproduced well. But other features of the lattice like window size and diffusion properties in this system must also be taken into account.

This work has used most of the force field parameters Hertäg et al. [19] to describe flexibility of the lattice. Detailed discussions of these parameters and tables with the parameter values used in this work are given in appendix A.

##### 3.1.1 General features of the simulations

All MD simulations reported in this paper were done using the DL\_POLY program, version 2.20 (see [68]). Ewald summation was applied for the electrostatic fields that are connected with the particle charges. Interaction parameters are given in the appendix A.

In this work the parameter sets for flexible ZIF-8 from Hertäg et al. [19], Zheng et al. [35] and Zhang et al. [36] are compared. The C<sub>2</sub>H<sub>6</sub> molecule has been described by the transferable potential for phase equilibria (TraPPE, Martin et al.) [69]. The nonpolar C<sub>2</sub>H<sub>6</sub> molecule is modeled in this paper by two united atoms (CH<sub>3</sub> groups) connected by a rigid bond. The parameters for N<sub>2</sub> have also taken from the transferable potential for phase equilibria (TraPPE) but from Potoff et al. [70]. This

force field describes nitrogen by 3 force centers namely the two N atoms and a fictive charge center placed at the center of mass of the  $N_2$  molecule to ensure charge neutrality.  $N_2$  is a nonpolar molecule. The bond lengths between the 3 centers are fixed. Further details of the parameters used in the simulations are given in the appendix A.

### 3.1.2 Force field validation using isothermal-isobaric (NPT) ensemble

The ZIF-8 structure was taken from the XRD data of the Cambridge Crystallographic Data Center (CCDC) [8]. It contains 4- and 6-membered rings. The cubic framework of ZIF-8 consists of zinc and 2-methylimidazolate (2-MeIm) linkers with a lattice constant of 16.9910 Å as displayed in Figure 3.1.

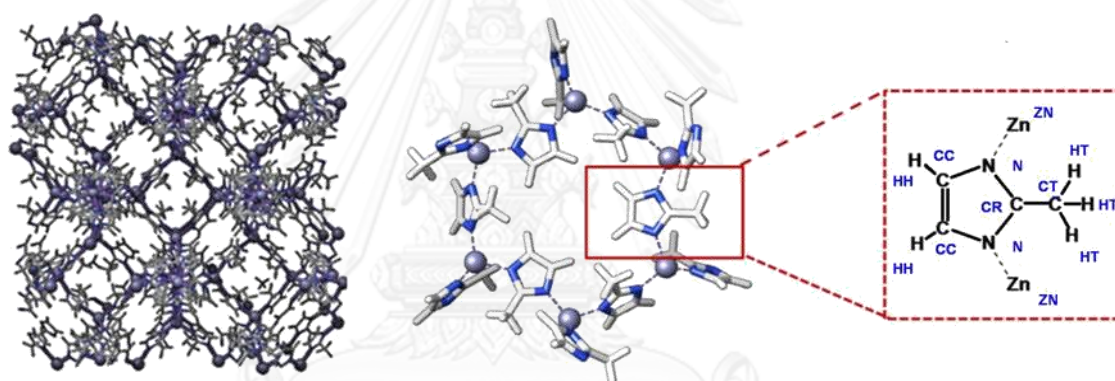


Figure 3.1 ZIF-8 structure. The 2x2x2 unit cells (left) and the 6-membered pore aperture with six 2 methyl-imidazolate linkers and six Zn<sup>2+</sup> ions (right).

MD simulations of the empty ZIF-8 framework were carried out in the isothermal-isobaric (NPT) ensemble. The simulation box contained 2x2x2 unit cells (initial size: 33.982 x 33.982 x 33.982 Å<sup>3</sup>). The six ZIF-8 parameter set models will now be considered. They will be named set A to F. Set A is the parameter set of Hertäg et al. [19]. In parameter sets B and C, the  $k_r$  of the Zn-N bond of [19] have been changed. In parameters set B,  $k_r$  is 80 and in set C it is 160 kcal/mol/Å<sup>2</sup>. The parameter set D essentially agrees with that of [19]. But, the charges of set D are taken from Zheng et al. [35]. Parameter set E is the set of [35]. The last one, parameter set F is the set of Zhang et al. [36]. The properties of the flexible ZIF-8 lattice will now be analyzed for set A to E considering the empty framework like in [35]. The temperature was  $T = 300$  K and the pressure was 6.022 atm. Moreover,

parameter set C and F were investigated both of empty ZIF-8 framework and ZIF-8 framework with  $N_2$  at different loadings between 0.5 and 30.0 molecules/cage. The system was examined at the two temperatures, 258 K and 300 K. The pressure was chosen to be 1 atm or zero to determine the box size of the frameworks, respectively.

All systems were allowed to equilibrate for 1 ns and then the evaluation part of the run was carried out for 2 ns. The cutoff for all LJ interactions was set to be 12 Å.

### 3.1.3 Dynamic properties of ethane molecules in ZIF-8 framework with different interactions

The simulations have been done at a concentration of 2.5 molecules/cage for the parameter sets A to D to check which parameter set is the best one for the examination of diffusion of  $C_2H_6$  in ZIF-8. All frameworks are flexible throughout the simulation. The numbers of unit cells in these simulations were 2x2x2 (that means an edge length of the box of 33.982 Å). Periodic boundary conditions were used. The temperature was set equal to 300 K and the pressure was 1 atm. The simulations were now first performed in the isochoric-isothermal ensemble (NVT) to equilibrate the system for 5 ns. Then, the evaluation run of 50 ns was carried out in the micro-canonical ensemble (NVE). Equilibration was done for 0.5 ns. The time step was 2 fs. The cutoff radius of the LJ interactions was chosen to be 14 Å.

MD simulations the best of the parameter sets have then been done for different loadings between 0.5 and 15 molecules/cage. The results are compared with measurements of Bux et al. at 298 K. [71]. Bux et al. reported results from sorption uptake experiments of pure  $C_2H_6$  on large ZIF-8 single crystal and GCMC supported IR microscopy (GCMC-IRM). Moreover, data from MAS PFG NMR measurements [72] carried out for  $C_2H_6/C_2H_4$  mixtures have been compared also. Moreover, the numbers of  $C_2H_6$  molecules in the simulations was increased to check the influence of the guests on the window diameter of the 6-membered rings and density plots of the  $C_2H_6$  location in ZIF-8.

The diameter of the 6-membered window in the ZIF-8 lattice has been visualized by the yellow sphere in Figure 3.2. The diameter has been defined here different from the way that is done usually. Usually, the distance between opposite atoms in the window is considered. But also the shape of the opening should be taken into account. Therefore, in [19] the window diameter has been derived from



the diameter of the largest sphere that fits into the window. The technical details for calculation window diameter are described in appendix A.

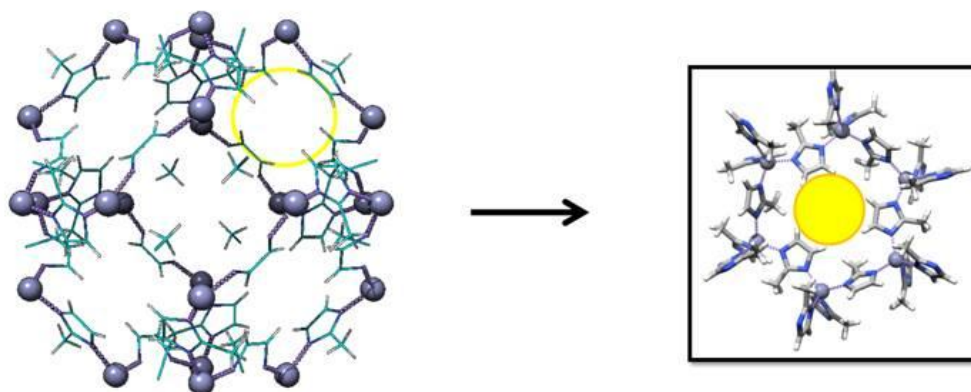


Figure 3.2 The 6-membered window of the ZIF-8 framework as estimated from XRD data [8] plus adding the hydrogen electron clouds which gives a diameter of 3.4 Å. A yellow sphere is visualizing the window size.

The simulation box consists of 2x2x2 unit cells that have 64 pore apertures over which the average was taken.

#### 3.1.4 Potential energy profile for an ethane molecule passing the window

To understand the self-diffusion of  $C_2H_6$  in ZIF-8, the energy profile for a  $C_2H_6$  molecule passing the ZIF-8 windows was investigated. The only way for a guest molecule to migrate from cavity to cavity is pass the 6-membered ring. The Figure 3.3 shows a snapshot was extracted from a MD trajectory of  $C_2H_6$  in ZIF-8. As a model one isolated 6-membered ring was observed. The potential energy of a  $C_2H_6$  molecule passing the window in the orientation illustrated in Figure 3.3 (all atoms are drawn small for clarity of the picture) was calculated for positions that are separated by shifts of 1 Å. Lattice fragment and  $C_2H_6$  molecule were kept rigid. The positions included an interval starting and ending at 7 Å distance from the center of the window as shown in Figure 3.3 (b). This molecular mechanics calculations were done by an own small FORTRAN program. The results can be found below.

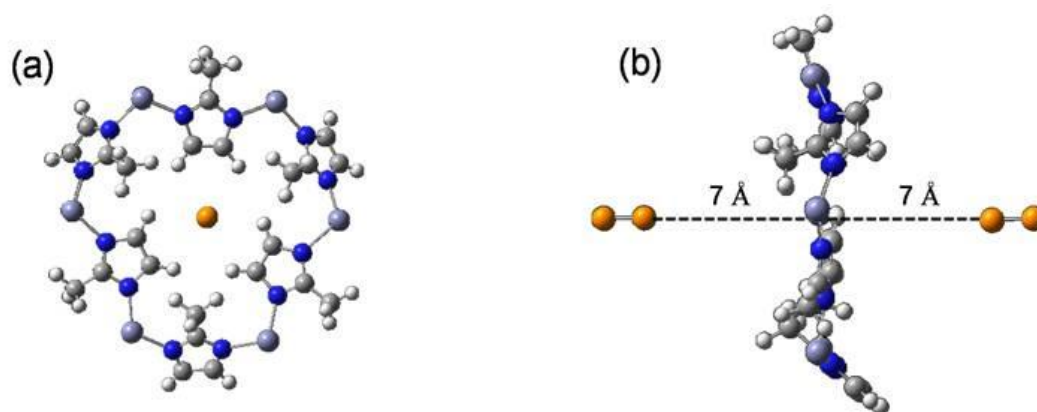


Figure 3.3 The arrangement used for the molecular mechanics (a) top view, (b) side view. The dumbbell represents the C<sub>2</sub>H<sub>6</sub> molecule.

### 3.1.5 Structure of the flexible ZIF-8 framework and dynamic properties of N<sub>2</sub> within ZIF-8 framework with various interactions

A geometric parameter that is very important for diffusion. The window diameters of the 6-membered rings in ZIF-8 at 258 K (temperature of the X-ray experiment in [8]) and 300 K (room temperature) from MD simulations by using parameter set C and F are compared with the window diameters of the 6-membered rings in ZIF-8 from X-ray diffraction data. These simulations of flexible ZIF-8 frameworks were started in the NVT ensemble to equilibrate the system for 5 ns and then allowed to equilibrate for another 0.5 ns in the NVE, followed by the production run of 5 ns (NVE). The time step was set to 1 fs. The unit cell size in our NVE simulation is the same as in the XRD data.

Again, the flexible ZIF-8 frameworks were studied at N<sub>2</sub> loadings between 0.5 and 30.0 molecules per cage for parameter set C and F. These parameter sets were used to determine the window diameter of 6-membered rings of ZIF-8 and the self-diffusivity of N<sub>2</sub> in ZIF-8. The temperature in the simulation box was set to 300 K. To shed light on the mechanism of the gate-opening on an atomic level, the window diameter of the 6-membered rings of ZIF-8 is compared with the self-diffusivity of N<sub>2</sub> molecules and density plots of the N<sub>2</sub> location and the radial distribution functions in ZIF-8 with the appropriate parameter set.

### 3.2 Quantum chemical calculations

The heavily discussed gate-opening is often thought to be a saloon door-like rotation of the linker in ZIF-7 or ZIF-8. To check this the configurational energies for different orientations of the linker have been calculated using ab initio calculations at B3LYP-6-31G(d) level including LANL2DZ. Figure 3.4 and 3.5 show the part of the ZIF-8 that was considered (highlighted). The calculations were done by the GAUSSIAN software package [73].

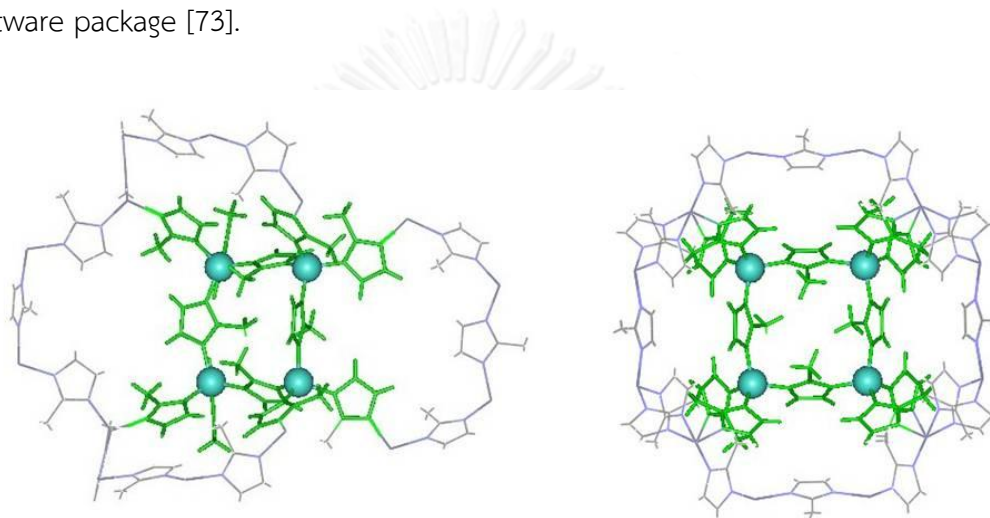


**Figure 3.4** Different views of the part of 4-membered ring in the ZIF-8 lattice that formed the model for the quantum mechanical calculations.

In Figure 3.4, the region in between four windows (the 6-membered rings are right, left, above and below from the highlighted region) is examined. The investigations (i) Rotation of only one linker (the central one in Figure 3.4, left or middle picture) and (ii) Simultaneous rotation of all linkers of the 4-membered ring (Figure 3.4) in order to investigate correlations among linkers. The 4 member ring was chosen because a more pronounced correlation effect was expected than in the 6-membered ring (window). Rotation of the 4-membered rings in the range of  $0^{\circ}$ – $360^{\circ}$  was computed every  $30^{\circ}$ . After that, the energies in the range of  $0^{\circ}$ – $30^{\circ}$  with an interval of  $5^{\circ}$  have been calculated.

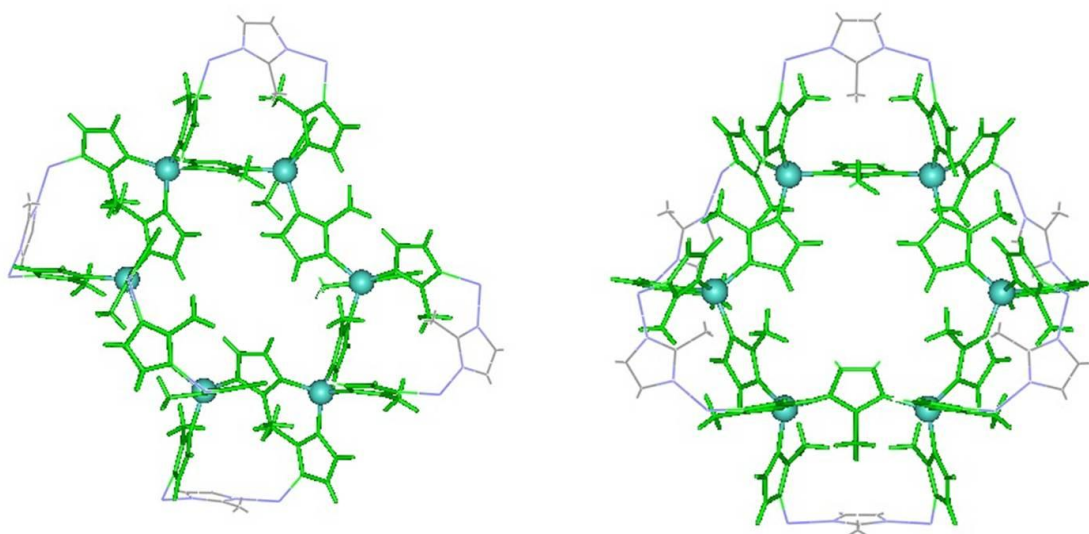


Figure 3.5 Different views of the model part of 6-membered ring used in the quantum mechanical evaluations.

In Figure 3.5 the region between six windows is displayed (the 4-membered rings are right, left, above and below from the highlighted region). Due to the number of atoms in the system is too large. Therefore, only one linker has been rotated in the interval  $0^{\circ}$ – $360^{\circ}$  by steps of  $30^{\circ}$ .

## CHAPTER IV

### RESULTS AND DISCUSSION

#### 4.1 Molecular dynamics (MD) simulations for $C_2H_6$

In this part, the MD simulations are done to study force fields of Hertäg et al. [19] and Zheng et al. [35] in the NPT ensemble to investigate the unit cell size of flexible ZIF-8 of these parameter sets and in the NVE ensemble in order to compare the lattice geometry and mobility of guest molecule. Moreover, the present section contains the examination of the migration of  $C_2H_6$  molecules and their influence on the ZIF-8 lattice.

##### 4.1.1 Framework properties for different force fields

The force fields for the flexible ZIF-8 by Hertäg et al. [19] and Zheng et al. [35] were studied. The bond elastic energies ( $U_{bond}$ ) as a function of the bond length of the Zn-N bond for the two systems, as calculated by equation 1 in appendix A can be seen in Figure 4.1.

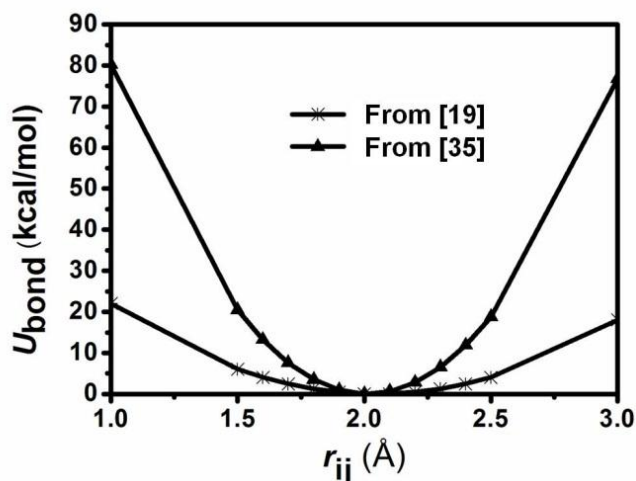


Figure 4.1 Potential ( $U_{bond}$ ) for the vibration of the Zn-N bond (harmonic oscillator) calculated from the force field parameters used from refs [19] and [35].

The parameter sets for the ZIF-8 from references [19] and [35] will now be compared. The differences in the  $k_r$  for the Zn-N interaction (Table A.1) and the partial charges (Table A.6 of the appendix) between both parameter sets are crucial. They cause the different box sizes in the simulations. The bond potentials ( $U_{\text{bond}}$ ) of Zn-N bond for two systems are shown in Figure 4.1. The  $U_{\text{bond}}$  from ref [19] is drastically weaker than that of ref [35]. Hence, the parameters from ref [19] lead to a more flexible lattice. Even though, the force field from ref [35] can remain the box size of the ZIF-8 system in NPT simulations compared to the experimental XRD structure better than that of ref [19], other size parameters like the window shape should be checked taking into account that in [19] the  $\text{H}_2/\text{CH}_4$  selectivity in ZIF-8 can be modeled very well in agreement with the experiment.

The empty ZIF-8 lattice has been checked in the NPT ensemble, in order to investigate the behavior of the lattice geometry during the simulations. The box size and the Zn-N bond lengths have been compared with the experimental data. The results for systems (A-E) are shown in Table 4.1

**Table 4. 1** The edge lengths of the MD boxes and the Zn-N bond lengths of ZIF-8 found in the MD simulations with NPT ensemble with the different parameter sets, respectively and differences from the XRD derived structure (box size: 33.982 Å and Zn-N bond: 1.987 Å). Note that the box lengths in x, y, and z directions are equal. The deviations from experimental XRD values are written in parenthesis.

Systems	$k_r$ for Zn-N (kcal/mol/Å <sup>2</sup> )	Box size (Å)	Zn-N (Å)
Parameter set A	40	29.790 (4.192)	1.662 (0.325)
Parameter set B	80	30.680 (3.302)	1.794 (0.193)
Parameter set C	160	31.370 (2.612)	1.912 (0.075)
Parameter set D	40	33.305 (0.677)	1.970 (0.017)
Parameter set E	157	33.165 (0.817)	1.985 (0.002)

In Table 4.1, the deviations of the box lengths from the XRD data are 0.677 - 4.192 Å. They are mostly significant for the Zn-N bond length, where they are 0.002-0.325 Å as shown in the parenthesis. This work considered the box sizes of the system A-C and D-E, which use also different partial charges. The box size is determined by the  $k_r$  constant of Zn-N bond, and by the partial charges. Using the partial charges from ref [35] very good agreement of the box size with that of the X-ray structure can be achieved. The results point to the importance of the  $k_r$  constant and the charge model for the structure.

#### 4.1.2 C<sub>2</sub>H<sub>6</sub> diffusivity in ZIF-8 framework

The self-diffusion of C<sub>2</sub>H<sub>6</sub> has been examined in the NVE ensemble because *e.g.* in the NVT ensemble well known artifacts can appear. In most thermalization procedures the temperature is maintained by scaling of the velocities of the atoms. This can create nonequilibrium situations including different temperatures for different degrees of freedom of the molecules.

Nevertheless, the system can be thermalized in an initial NVT run if it is then relaxed to equilibrium before the evaluations start. During the evaluation part in the NVE ensemble the temperature was only slightly fluctuating within about one per cent around 300 K. No thermalization was therefore needed.

The mean square displacements (MSDs) of C<sub>2</sub>H<sub>6</sub> molecules in the ZIF-8 lattice at 300 K and loading of 0.5, 2.5, 5, 7.5, 10, 12.5 and 15 molecules/cage, were calculated over 20 ns. The self-diffusion coefficient ( $D_s$ ) of the C<sub>2</sub>H<sub>6</sub> molecules was calculated using the Einstein formula from the MSDs. The MSDs of the C<sub>2</sub>H<sub>6</sub> molecules in the flexible ZIF-8 lattice at loading of 2.5 molecules/cage for systems A-E can be seen in Figure 4.2 (left). The  $D_s$  values fitted from the MSDs for system A, B, and C were found to be  $6.02 \times 10^{-11}$ ,  $5.99 \times 10^{-11}$  and  $5.85 \times 10^{-11}$  m<sup>2</sup>/s, correspondingly. The order of magnitude of the results agrees with experimental transport diffusivity ( $D_T$ ) at 298 K [71], which were obtained from the C<sub>2</sub>H<sub>6</sub> in ZIF-8 single crystal by IRM detection [72].

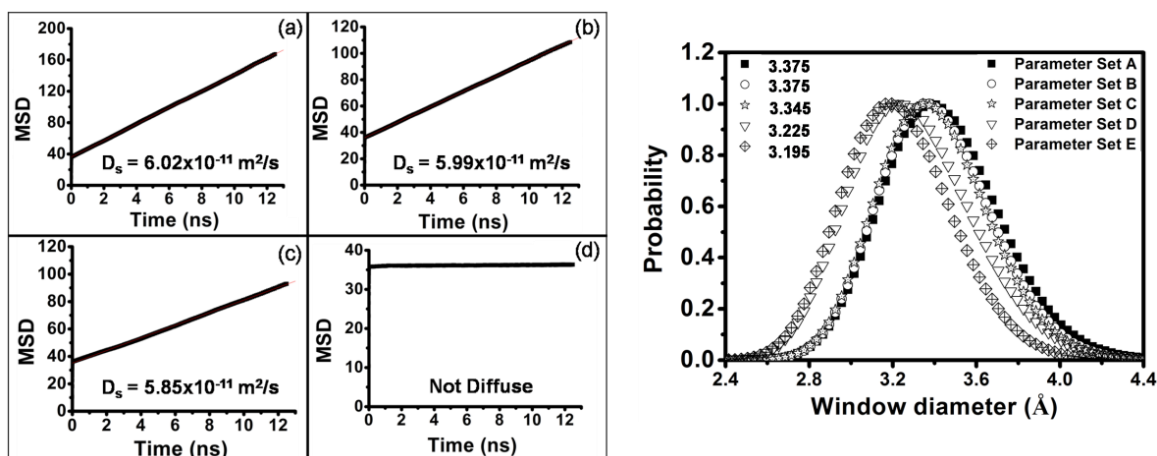


Figure 4.2 (Left) The mean square displacements (MSDs) of  $\text{C}_2\text{H}_6$  molecules in ZIF-8 at loading of 2.5 molecules/cage and the obtained self-diffusion coefficients ( $D_s$ ) for system A (a), system B (b), system C (c), and systems D and E (d). (Right) The distributions of the window diameters from the simulations of 2.5 molecules/cage for all parameter sets.

The mobility of guest molecules is determined essentially by their ability to pass the windows. Hence this work also studied the diameter of the 6-membered ring windows through which molecules must pass to proceed from one cavity to the next one. The window diameters achieved from the maximum of the diameter distributions for systems A, B, C, D, and E are 3.375, 3.375, 3.345, 3.225 and 3.195 Å, respectively as shown in Figure 4.2 (right). Using the interaction parameters from D and E sets the window sizes are smaller than the experimental ones obtained from XRD data. The window size essentially determines the diffusion performance of  $\text{C}_2\text{H}_6$  molecules.

It becomes apparent that the  $D_s$  of  $\text{C}_2\text{H}_6$  molecules in systems D and E are negligibly small. That means that  $\text{C}_2\text{H}_6$  molecules would not diffuse in ZIF-8 in contradiction to experiments. This is due to the smaller windows for these parameter sets. This results from the conformation of the ZIF-8 linkers which are different from the XRD structure. By the parameter sets D and E, the linker-turning leads to narrow windows. The superimposition of the 6-membered ring from snapshots of MD runs by systems A and D at loadings of 2.5 molecules/cage and that from XRD are visualized in Figure 4.3.



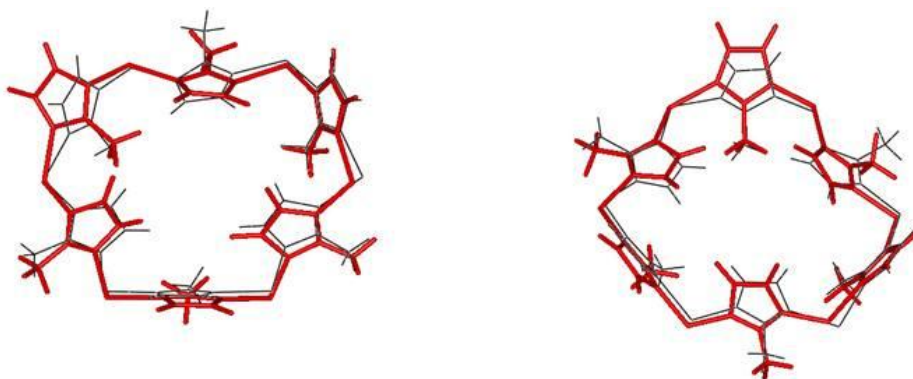


Figure 4.3 Superimpositions of the 6-membered ring from XRD (black) and that from the simulations of ZIF-8 lattice with  $C_2H_6$  molecules (red) for the parameter sets A (left) and D (right).

#### 4.1.3 Influence of the concentration of $C_2H_6$ on the self-diffusion coefficient and the windows size

As outlined in section 4.1.2 only the parameter sets A, B, and C yield realistic  $D_s$  values. To compare  $D_s$  for different force constants of the Zn-N bond on, the parameter sets A and C were selected. The loading dependence of  $D_s$  of  $C_2H_6$  in ZIF-8 is shown in Figure 4.4.

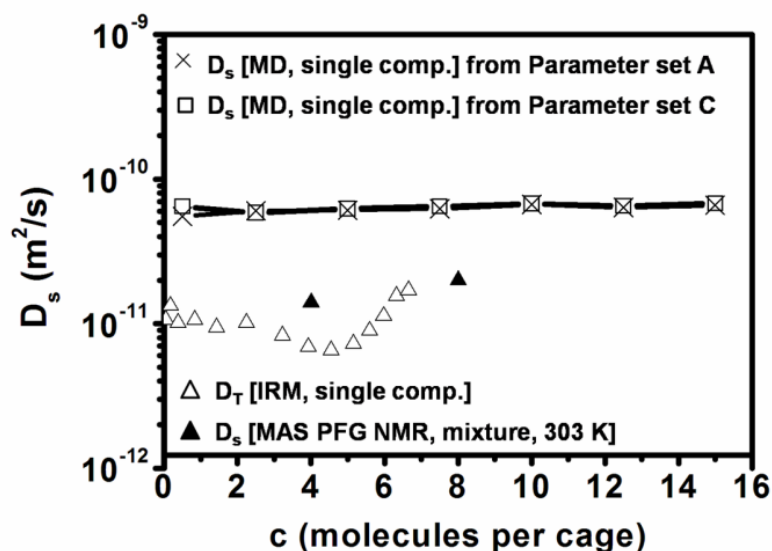


Figure 4.4  $D_s$  for  $C_2H_6$  in a ZIF-8 for the parameter sets A and C as function of loading (see appendix B in Table B.1) compared with experimental results.  $D_s$  values from IRM are calculated from  $D_t$  values as expressed in [71].

The  $D_s$  values from MD are approximately not different for the parameter sets A and C. However, the  $D_s$  are larger than those obtained from sorption uptake/desorption experiments with IR detection [71, 72]. This is quite frequently the case in such comparisons of MD and experiment. This disagreement can be caused by reduced diffusion in real crystals because of lattice defects, grain boundaries, pore blocking *etc.* Instead the crystal of the MD simulation is perfect. This is true for all kinds of classical molecular simulations if the parameters are not fitted to experiments. In [74] for the adsorption of *e.g.* CH<sub>4</sub> and CO<sub>2</sub> in ZIF-68 and ZIF-69 the hypothesis of partial pore blocking was checked. Blocking some pores randomly one choice of blocking gave very good agreement of simulations with experiment using unfitted generalized force field parameters. It is clear that pore blocking would decrease the diffusivity.

Possible reasons for the low loading-dependence of the self-diffusivity found in our results and also experiments (Figure 4.4) will be discussed in the next section.

Figure 4.5, shows that the window diameter became smaller with increasing loading from 0.5 to 16 C<sub>2</sub>H<sub>6</sub>/cage.

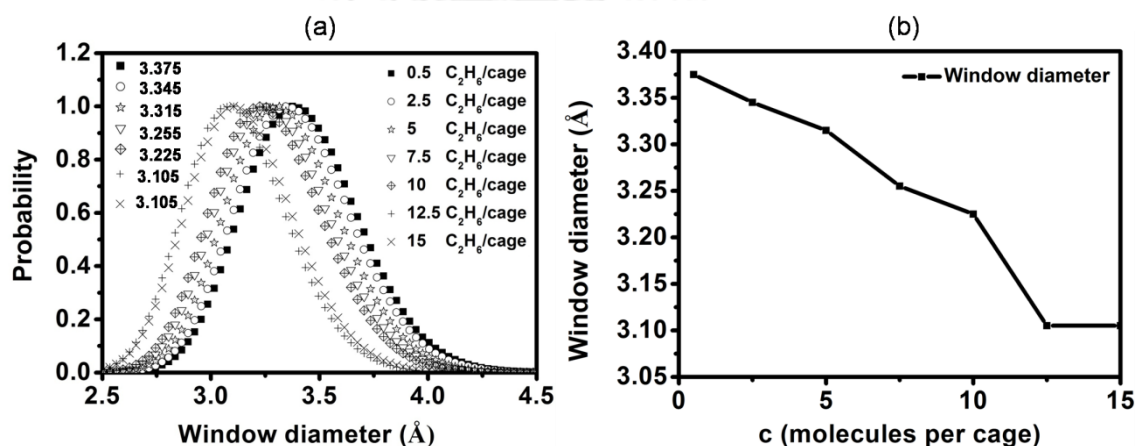


Figure 4.5 (a) Windows diameter distributions as function of loadings with C<sub>2</sub>H<sub>6</sub> achieved from the sets A and C (the results for the parameter sets A and C are nearly the same). (b) Average window diameters gained from snapshots from trajectories from parameter set C.

Surprisingly, the reduction of the window sizes with increasing loading does not affect the  $D_s$  much as shown in Figure 4.5. To understand this discovery, the potential threshold in the window will be discussed in the next section.

#### 4.1.4 The potential threshold in the window

The local Helmholtz free energy [75], (that is the potential of the average force on a given probe molecule at a given position [76]) would be very helpful to understand the results of section 4.1.3. With its help even Transition State Theory could be used to calculate transition probabilities for the passage of the window [77]. By umbrella sampling this would be possible with reasonable effort for a rigid lattice along the so called MEP (minimum energy path), the most probable path for passing molecules. Unfortunately, in the vibrating lattice there is no permanent MEP. Instead it will depend on time making its estimation difficult. This evaluation is time consuming to be done in the present work.

The mentioned probe particle shifting will now be applied to study the particle migration in detail. For randomly chosen situations (snapshots) from MD trajectories the potential energy of a fictive  $C_2H_6$  test molecule is calculated for a sequence of positions along the central line throughout the window. The test molecule will be always be directed parallel to this line. The positions of lattice atoms and (real) guest molecules are fixed. Every atom and molecule exerts forces on the test molecule. This should give a realistic picture of the potential landscape for the fictive test molecule. Note, that in reality, only orientations of the  $C_2H_6$  molecules close to the mentioned one will allow passage of the window. The special choice of the snapshot will, of course, influence the results.

For comparison the energy values are shown in the pictures as differences to the minimum energy along the on the path. The energy unit is kcal/mol. The energy barriers were found to be notably different between systems A and D whereas sets A and C are very similar to each other. The energy barrier for system A is only 5.98 kcal/mol while for system D it is up to 17.81 kcal/mol. The comparison of the thresholds may explain why the  $C_2H_6$  molecules can only diffuse in systems A or C, but not in system D because its barrier is much higher. For the difference between sets A and C note that each of these two evaluations have been done using an arbitrarily chosen single snapshot from the corresponding trajectory thus fluctuations must be taken into account. The variation is within the range of such fluctuations.

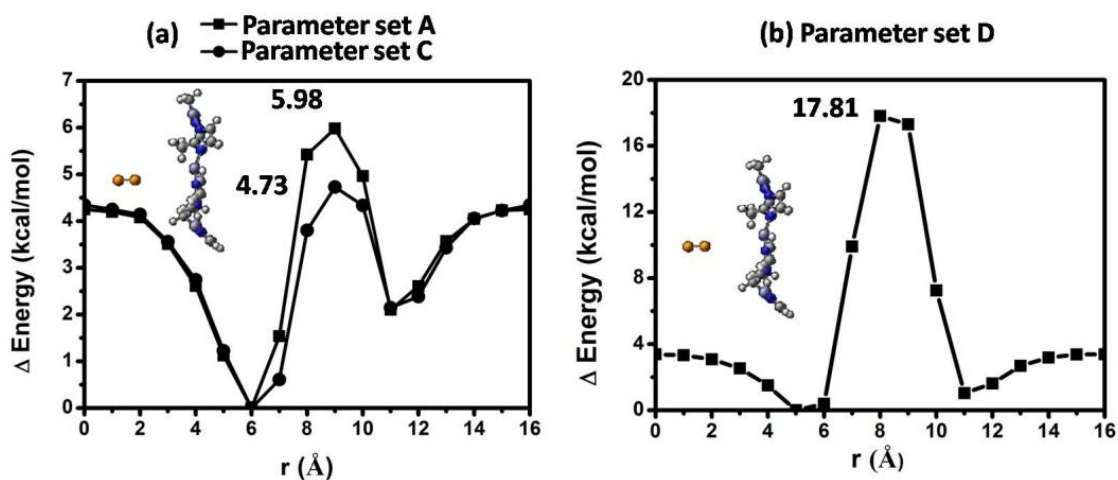


Figure 4.6 The energy barriers for  $C_2H_6$  molecule obtained as described in the text for parameter sets A, C and D (see in Figure 4.2 right). The loading was 2.5 guest molecules/cage at 300 K. Note, the insets shall only demonstrate the geometry of the arrangement and do not represent the real atom sizes.

Because the window size is better reproduced with parameter sets A and C than with set B or D and the diffusion of the  $C_2H_6$  is possible with parameter sets A and C like it is in the experiment these parameter sets have been chosen. The deviation of the cell size in NPT simulations for the parameter sets A and C from XRD data are not important because we have done the simulations in the NPT ensemble. Thus the unit cell size is constant and in exact agreement with XRD data.

Parameter set C which shows the lowest decrease of the box size in NPT was finally used for the examination of the window size as a function of the  $C_2H_6$  loading in Figure 4.5(b). Modification of the bond parameter like in set C is also used in [20] and [35] where also a stronger bond parameter than that from generalized force fields has been introduced empirically in order to maintain the unit cell size closer to the value from XRD data.

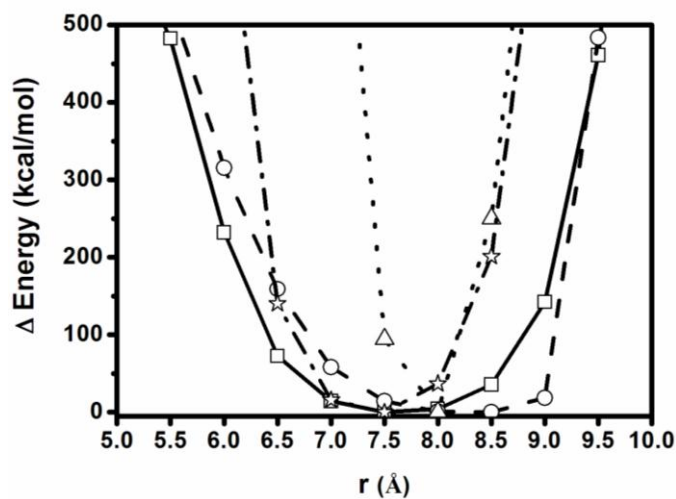


Figure 4.7 The potential energy profile for  $C_2H_6$  probe molecule passing the ZIF-8 window for the parameter set C at a loading of 15 molecules/cage at 300 K. The states are selected randomly from one trajectory in which no other  $C_2H_6$  is within the window region.

Though the window diameter for 12.5 and 15 molecules/cage is of the order of only 3.1 Å while it was 3.35 Å for lower concentrations  $D_s$  is nearly the same. Figure 4.7 shows a possible explanation why the  $C_2H_6$  molecules quite often pass the smaller windows at high loadings. The potential energy profiles for a  $C_2H_6$  molecule at the loading of 15 molecules/cage has been evaluated for some snapshots in which there is no other  $C_2H_6$  in the window region. It can be seen that outside of the window there are enormous potential gradients (forces) toward the window. The other  $C_2H_6$  molecules around the window press the test molecule into the window. This discovery fits well to the fact that snapshots with no  $C_2H_6$  molecule in the window are very rare.

The explanation for the almost constant self-diffusion coefficient  $D_s$  is that the influence of the other  $C_2H_6$  molecules on the test molecule compensates the smaller window size at high loading.  $D_s$  is even slightly increasing with loadings for the examined densities. For very high loadings it must tend to zero, of course.

## 4.2 Molecular dynamics (MD) simulations for $N_2$

In this part the interplay of structural properties and self-diffusion of  $N_2$  molecules will be examined by using the parameter set C as suggested in  $C_2H_6$  (section 4.1). This parameter set is able to explain the structural change in the ZIF-8

lattice induced by the  $N_2$  adsorption (as found in experiments and other simulations [34, 36] and compare the predictions for the guest dynamics with the values obtained using the parameter set F suggested in Zhang [36]. NPT simulations have been done for the comparison of different parameter sets on the ZIF-8 lattice structure whereas the investigations of the structural and diffusion properties have been carried out in the NVE ensemble.

#### 4.2.1 Force field validation for the flexible ZIF-8 framework at 258 K and 300K by NPT ensemble

The unit cell size is frequently used to validate the force field in NPT. Although, as mentioned there are more important criteria as explained in section 4.1, in this section MD simulations of the empty ZIF-8 framework have been carried out under the NPT ensemble, pressure zero, in order to investigate the box lengths of the framework during the simulations using parameter sets C and F. The simulation boxes from MD calculations at 258 K and 300 K were compared with the experimental data of Park et al. (258 K) [8] as shown in Figure 4.8.

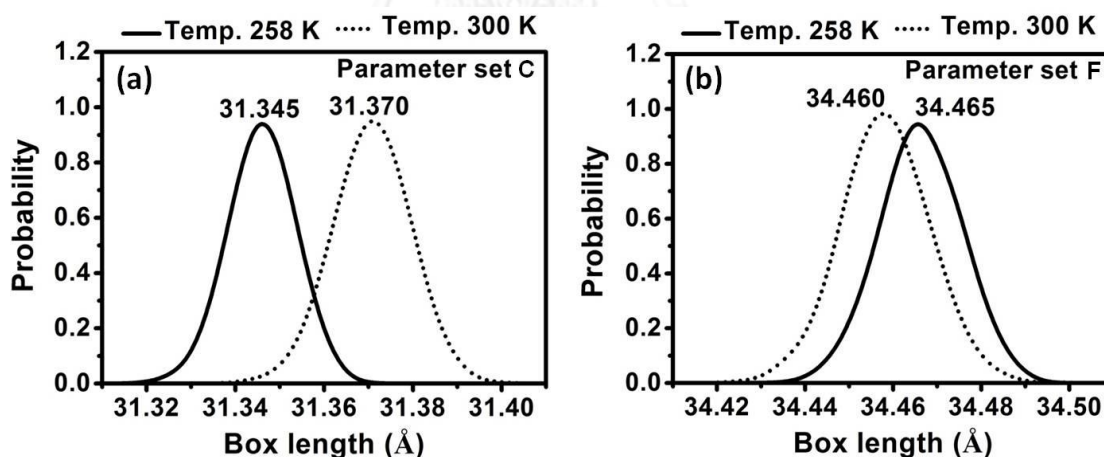


Figure 4.8 The box size distributions of ZIF-8 framework at 258 K and 300 K achieved from the MD simulations under the NPT ensemble (a) Parameter set C and (b) Parameter set F.

In Figure 4.8, the dimensions of the simulation box of ZIF-8 calculated for parameter set C and F are dissimilar from the XRD data (33.982 Å). For parameter set C, the simulation boxes at 258 K and 300 K were found to be 31.345 and 31.370 Å, correspondingly. For parameter set F, the simulation boxes at 258 K and 300 K were found to amount 34.465 and 34.460 Å, correspondingly. The slight difference of the maximum position for set F in Figure 4.8 (b) of 0.005 Å in the two different MD runs respectively, is  $1.45 \times 10^{-4}$  of the box size and is below the limit of adjustment. Therefore, the temperature dependence of the box size is too small to be calculated in this way. Parameter set F could reproduce the size of the ZIF-8 unit cell given in XRD data [8] with decent accuracy. Clearly, parameter set C leads to a too smaller unit cell size in comparison to the XRD data ( $33.982 - 31.345 = 2.637$  Å).

However, the simulation box size in NPT is not the only condition for choosing a parameter set for the simulation of diffusion. Principally, it is unimportant if the simulations are done in the NVE ensemble and not in NPT. The more important size of the windows connecting adjacent cavities and limiting diffusion will be discussed in the following section.

#### 4.2.2 Force field validation for the flexible ZIF-8 framework with N<sub>2</sub> loading at 300K by NPT ensemble

The flexible ZIF-8 framework with N<sub>2</sub> loading (between 0.5 and 30.0 N<sub>2</sub>/cage) at 300 K with 0 atm for low loading (0.5 to 18.44 N<sub>2</sub> molecules per cage) and 1 atm for high loading (24.69 to 30.0 N<sub>2</sub> molecules/cage) were also examined in the NPT ensemble using parameter sets C and F. The changes in the box dimensions of the parameter sets C and F are compared in Figure 4.9.

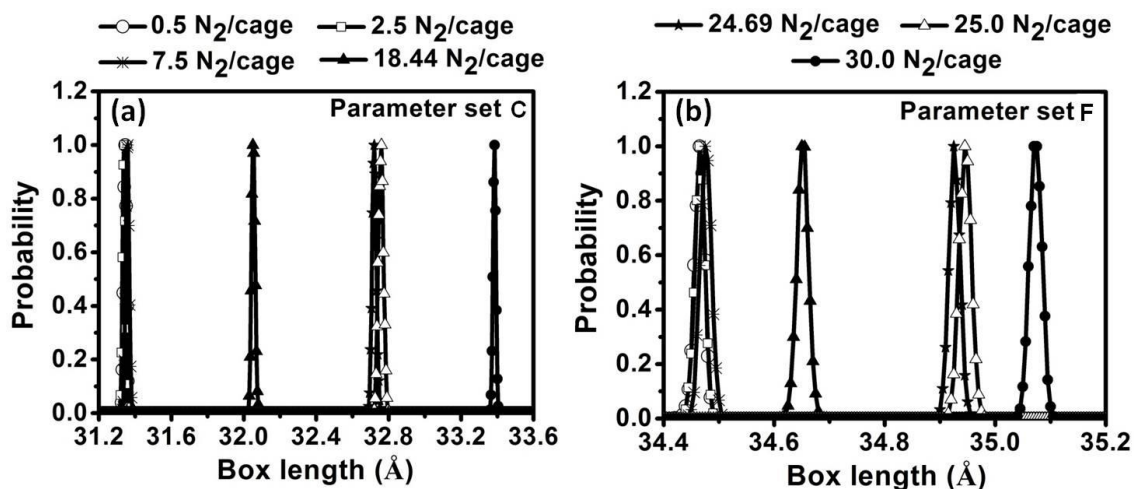


Figure 4.9 The box length distributions of ZIF-8 within N<sub>2</sub> loading at 300 K acquired from the MD simulations under the NPT ensemble with (a) Parameter set C and (b) Parameter set F.

For both parameter sets, the initial box sizes were set to 33.982 Å, in agreement with the XRD data. Afterward, it relaxed during the equilibration runs to the numbers given in Figure 4.9. For the parameter set C, the box length has been especially increased to 31.369, 31.365, 31.395, 32.115, 32.795, 32.850 and 33.455 Å with increasing N<sub>2</sub> loading at 0.5, 2.5, 7.5, 18.44, 24.69, 25.0 and 30.0 N<sub>2</sub>/cage, respectively. While parameter set F, the box size somewhat increases to 34.599, 34.465, 34.485, 34.685, 34.980, 35.00 and 35.145 Å with increasing N<sub>2</sub> loading of 0.5, 2.5, 7.5, 18.44, 24.69, 25.0 and 30.0 N<sub>2</sub>/cage, correspondingly.

Thus parameter set C predicts a sudden increase in the cell parameters once a loading of 18.4 molecules per cavity is crossed. This is the accurate loading where the gate-opening effect has been found in experiments [34]. This result provides a first indication, that also set C is able of capturing the gate opening effect in MD simulations. In section 4.2.1, it was found that parameter set C returns cell size parameters which are somewhat too small in NPT. But, as discussed, all further investigations were done in the NVE ensemble.

#### 4.2.3 Flexible ZIF-8 framework and N<sub>2</sub> dynamics investigated in the NVE ensemble

The cell size in NVE simulations is an input parameter and constant and exact by definition. This denotes that in NVE small fluctuations of the total simulation cell



box size are suppressed. Nonetheless, since the simulation box contains 8 unit cells, the cell size of each individual unit cell can still fluctuate. When it comes to the dynamics of diffusing guest molecules, geometry and the size of the windows connecting adjacent cavities is by far more essential than small deviations in the total size of the MD box. This bottleneck must be passed by the diffusing particles. Thus, the bottleneck permits some guest particles to pass whereas others cannot. The reproduction of this important feature is discussed in this section.

Therefore, this section is focused on the window size to validate the force fields for analysis of ZIF-8 framework and  $N_2$  dynamic properties in the NVE ensemble. The box size is fixed at the experimentally measured assessments. The window diameters of the ZIF-8 framework for parameter sets C and F at 258 K and 300 K are shown in Figure 4.10.

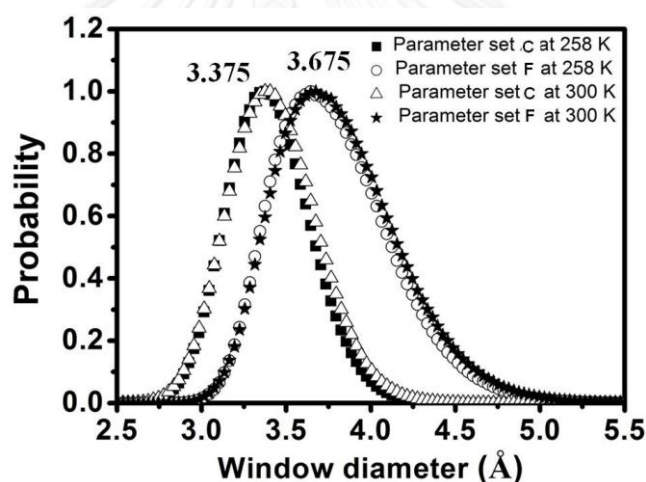


Figure 4.10 Distributions of ZIF-8 window diameters at 258 K and 300 K for parameter sets C and F.

The window diameters obtained from the maxima of the distributions for parameter sets C and F are 3.375 and 3.675 Å, respectively. The FWHM (full width at half maximum) of all curves is larger than 0.6 Å, demonstrating the obvious flexibility of the windows, which allow the passage of molecules with a size notably above the XRD window size (3.4 Å). Fascinatingly, for both sets the window diameter did not change with temperature. For parameter set C, the window diameter of the 6-membered rings is in outstanding agreement with the experimental XRD data (3.4 Å), while parameter set F overestimates the window size by approximately 0.3 Å. As a result, parameter set C appears to be more appropriate than parameter set F to

reproduce dynamic properties of guest molecules, as in pore systems with larger cavities framework by narrow windows of similar size as the diffusion molecules generally the window size dictates the molecular mobility.

XRD experiments evidenced a relocation of the linker molecules happening at higher  $N_2$  loadings [34]. Both parameter sets C and F predict a change in the box size at the proposed loading in NPT simulations, this section also expect to discover a sudden increase in the window size if the “gate-loading” loading is exceeded and this happens also in NVE simulations. Actually, such changes are observed for both parameter sets at 300 K (see Figure 4.11a) in NVE simulations.

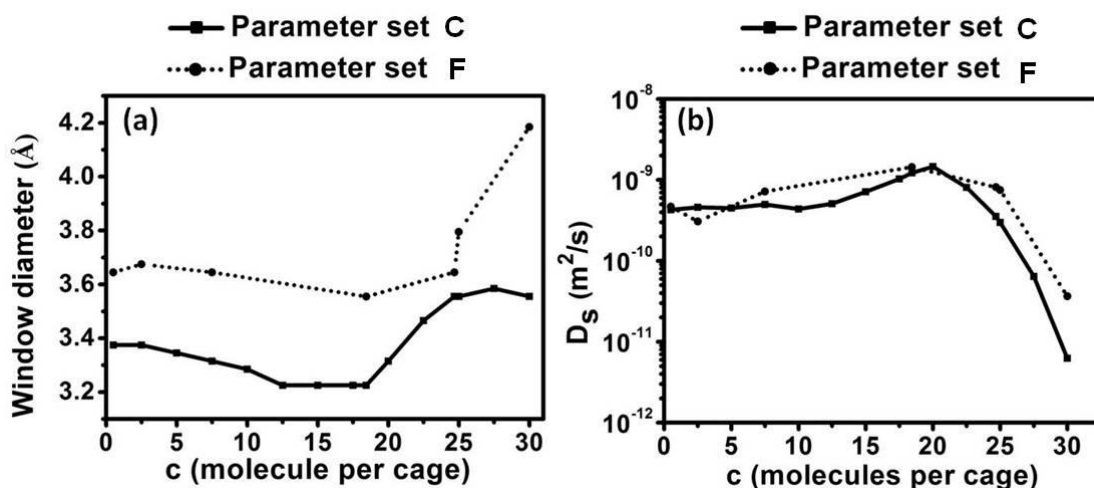


Figure 4.11 (a) Window diameters and (b) self-diffusivity  $D_s$  (see in appendix B in Table B.2) for  $N_2$  molecules within ZIF-8 framework for the parameter sets C and F.

Both parameter sets show a slight decrease in the window size as the loading is increased from zero to 18.44 molecules/cage, followed by a substantial increase afterwards by 0.36 Å for set C and 0.58 Å for set F, correspondingly. Whereas in set C this increase proceeds gradually as the loading rises from 18.44 to 24.7 molecules/cage, set F shows a steep increase only when the loading crosses 24.7 molecules/cage. With representing a transition point for a structural change near to a concentration of 18.44  $N_2$  molecules/cage, set C matches closely the gate-opening loading found in experiments by Fairen-Jiminez et al. [34]. The structural change resembles exactly the change of the ZIF-8 framework from the close to the open form as discussed in next section as same as observed by Fairen-Jiminez [34] and

Zhang et al. in [36] at 77 K. In comparison to Figure 4.10, the distributions of the window size for set C in dependence of the loading is displayed in Figure 4.12

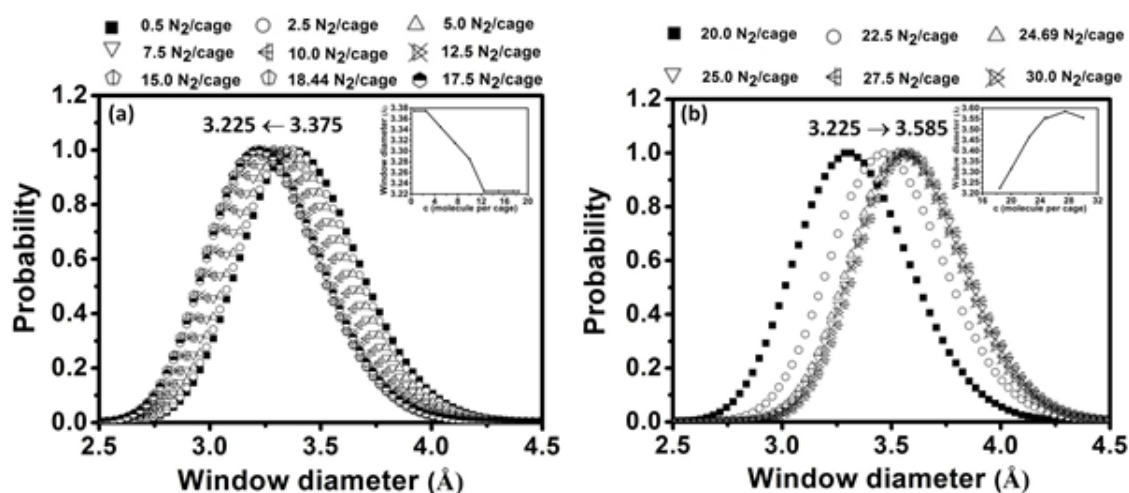


Figure 4.12 Distributions of ZIF-8 window diameters for different N<sub>2</sub> loadings at 300 K for parameter set C. (a) N<sub>2</sub> loading from 0.5-18.44 molecules/cage (b) N<sub>2</sub> loading from 20.0-30.0 molecules/cage.

Figure 4.12 shows the decreasing window diameters for loadings from 0.5 to 18.44 N<sub>2</sub> molecule/cage, where the window diameters dropped from 3.375 to 3.225 Å. After that, the loading increases from 18.44 to 30.0 N<sub>2</sub> molecules/cage, the window diameter increases from 3.225 to 3.585 Å. Fascinatingly, the curves are shifted as a whole without a change in the FWHM. For this reason, the fluctuations in the window size occur independently of the rotation of the linkers. Most interestingly, the sudden change in the window size is not accompanied by an enhancement of the self-diffusivity (see Figure 4.11b). The  $D_s$  values from both parameter sets somewhat increase until a loading of 18.44 N<sub>2</sub> molecules/cage and amount between  $10^{-9}$  to  $10^{-10}$  m<sup>2</sup>/s. After that, the diffusivity begins to decrease and then go downs sharply by 2 to 3 orders of magnitude in the high coverage region between 25 and 30 N<sub>2</sub> molecules/cage. The reason for this strong decrease is basically that at very high loadings the mutual hindrance of the N<sub>2</sub> molecules becomes the dominating factor and powerfully decreases the mobility. The magnitude of the diffusivity is in agreement with experiments and simulations of other small molecules. For CH<sub>4</sub> and CO<sub>2</sub> self-diffusivities in the range of  $1-3 \times 10^{-10}$  m<sup>2</sup>/s were evaluated [77]. Studies based on molecular simulations with a flexible lattice show numbers in the range of  $10^{-11}$  to  $10^{-9}$  m<sup>2</sup>s<sup>-1</sup>, depending on the selected

set of parameters [19, 20, 77-79]. The mobility of H<sub>2</sub> or D<sub>2</sub> is mostly shown in the order of 10<sup>-9</sup> to 10<sup>-7</sup> m<sup>2</sup>/s [19, 78, 80]. As common characteristics one discovers a weak dependence of the self-diffusivity on loading. Values for N<sub>2</sub> drop in between the intervals reported for H<sub>2</sub>/D<sub>2</sub> and CH<sub>4</sub>/CO<sub>2</sub>, as supposed based on the kinetic diameter of these molecules. Furthermore, the trend of the loading-dependence for low-intermediate pore fillings agrees well with the results for other molecules. The counter-intuitive finding that the increase of the window size does not result in a corresponding speed-up in the molecular mobility will be examined in more detail in the next section.

Figure 4.11b also illustrates that the self-diffusion coefficients  $D_s$  from MD are almost equal for the parameter sets C and F despite of the notably different window diameters. N<sub>2</sub> is a small molecule and the correct window size is more significant for the diffusion of larger molecules.

#### 4.2.4 More detailed examination of the gate-opening effect

The structural transition monitored using parameter set C is illustrated in Figure 4.13. In (a) and (b) a projection of a whole cavity including the surrounding lattice atoms on a plane is demonstrated for the high density and the low density configuration, respectively. The two kinds of windows are shown by different colors. The re-orientation of the imidazolate linkers in the ZIF-8 framework from closed (Figure 4.13) to open form (Figure 4.13) is exactly the structural transform which has been found in the high-pressure experiment of Moggach et al. [32] and in the work of Fairen-Jiminez et al. [34] and Zhang et al. [36] for N<sub>2</sub> adsorption. The re-orientation of the linkers is easily recognized as both structures are superimposed (see close-up views of the 4- and 6-membered ring windows in Figure 4.13 c and d).

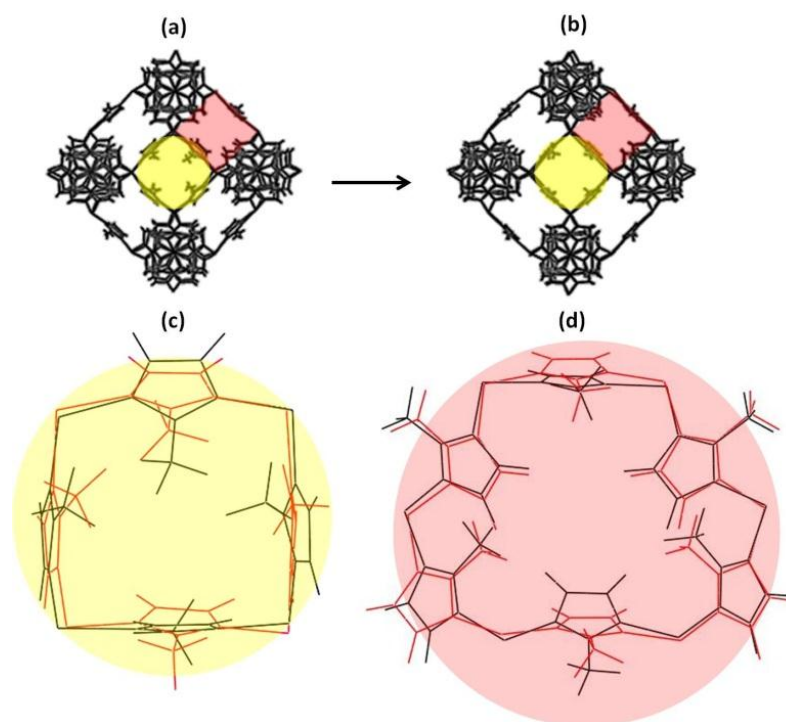


Figure 4.13 The transform of the orientation of the imidazolate linkers in the ZIF-8 framework for (a) low density (0.5 N<sub>2</sub>/cage) and (b) high density (15.0 N<sub>2</sub>/cage) N<sub>2</sub> loadings. Superimpositions of the low loading (black) and high loading (red) structures are shown for (c) the 4-membered ring and (d) the 6-membered ring.

To shed some light on the physics behind the loading dependence of the N<sub>2</sub> diffusivity this section considers in the following the probability density plots for the location of the N<sub>2</sub> molecules at different loadings as obtained from MD simulations using parameter set C at 300 K in the NVE ensemble (see Figure 4.14). The results are compared with the density plots for C<sub>2</sub>H<sub>6</sub>, as derived from the MD runs presented in the above section.

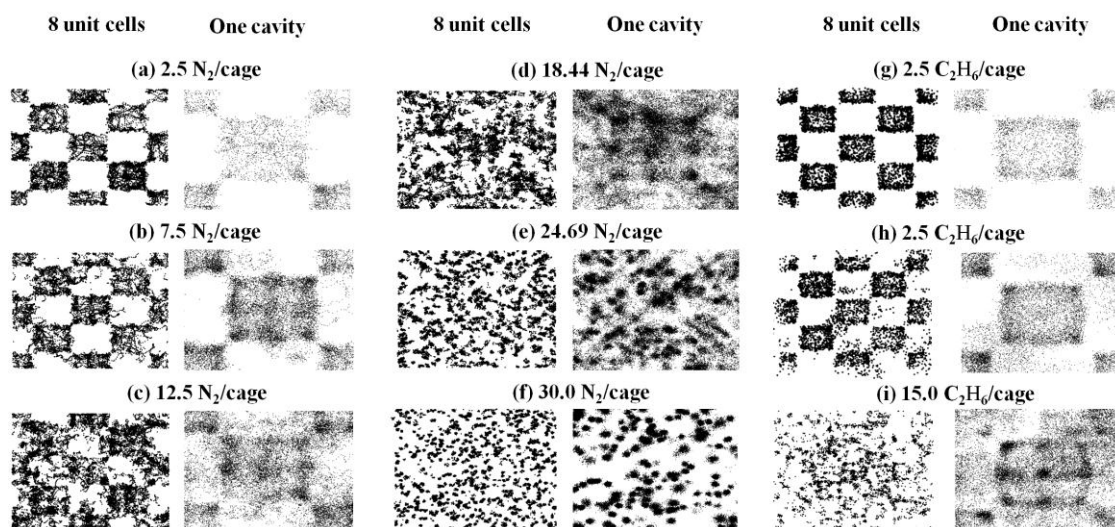


Figure 4.14 Comparison of the probability density plots for  $N_2$  and  $C_2H_6$  molecules at different loadings in ZIF-8. In each column the left hand picture shows a larger area whereas right hand picture shows the projection of a single cavity centered in the picture. Dark regions signify high probability density.

The plots illustrate the sites of the center of masses of the guest molecules at every 100 steps from the last 50000 steps of the production run in order to picture the probability density to find a particle at a given site. To support the interpretation of the density plots and why  $D_s$  decreased at high loading the radial distribution functions (RDFs) were determined in addition (see in Figure 4.15 and 4.16). The density plots at  $N_2$  loadings between 2.5 and 18.4 molecules/cage (Figure 4.15 a-d) illustrate a high density of  $N_2$  molecules in the funnel shaped entry region to the 6-ring windows and many  $N_2$  molecules passing the windows. The entrance region was also identified for  $CH_4$  and  $CO_2$  as preferred adsorption site [14] and also  $C_2H_6$  seems to prefer this region (Figure 4.14 g-h). As already stressed in [32] and [81] and proved in this RDF calculations (see in Figure 4.15), the structural transition at 18.4  $N_2$  molecules/cavity is accompanied by a packing rearrangement of the guest molecules. At the present, also sites near the 4-ring windows (see Figure 4.14) are populated which is only possible when the linkers are distorted. The linear shape of the  $N_2$  molecules together with the rearrangement then allows to contain more molecules in the cavities. The drastic change in the probability density plot at loadings above 18.4 molecules/cage (Figure 4.14 e and f) is a direct result of this more efficient packing. At high density, the next neighbors form a cage for each  $N_2$ . The picture shows similar to density plots of the phase transition in hard sphere or LJ

liquids. At high loadings, the RDFs reveal also a particularly strong interaction of the  $N_2$  molecules with the atoms at the CC and CT positions (Figure 4.15). Observably, the force constants describing the dihedral (stretching and bending) of the linker are of fundamental importance to capture the structural change in molecular simulations. In [36] it was concluded that their treatment of the dihedral of the imidazolate linker is comparable to the description of the dihedral (X-CT-CT-X) in the AMBER force field, in which CT are  $sp^3$  hybridized carbon atoms. Hence, in both of these simulations similar parameters are used for this dihedral elasticity which may explain partially why the gate opening effect is likewise expressed by both parameter sets.

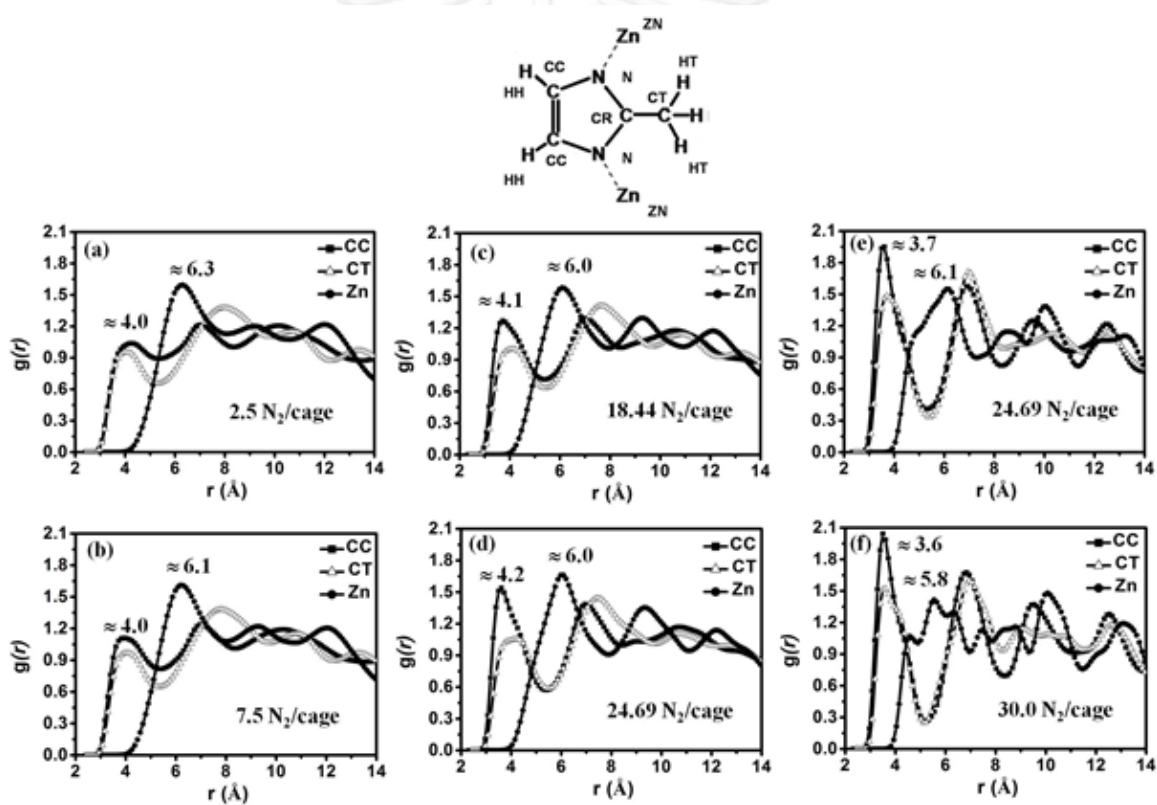


Figure 4.15 RDFs for a  $N_2$  molecule around the CC, CR, CT and Zn atoms in ZIF-8 framework at (a) 2.5  $N_2$ , (b) 7.5  $N_2$ , (c) 12.5  $N_2$ , (d) 18.44  $N_2$ , (e) 24.69  $N_2$  and (f) 30.0  $N_2$ /cage.

To confirm as mentioned above Figure 4.15 demonstrates the  $g(r)$  for  $N_2$  around the CC, CT and Zn atoms in ZIF-8 framework. At a loading 2.5, 7.5, 12.5 18.44, 24.69 and 30.0  $N_2$ /cage,  $N_2$  molecules were adsorbed close to CC and CT of the organic linker around a distance of 4.0 to 3.7 Å to the linker, whereas  $N_2$  molecules were located far from Zn clusters at distances of about 6.1 to 5.8 Å. These results show that the preferential adsorption site of the  $N_2$  molecule in ZIF-8 is the organic linker, similar to results presented in previous works [31, 82]. Thus,  $g(r)$  of the  $N_2$  molecules still remains large nearest to the CC and CT. With increasing number of  $N_2$  molecules/cage, sharp peaks are seen for  $N_2$  around CC, CT and Zn. Thus,  $N_2$  molecules have been found to have strong interaction with CC and CT at these positions. Additionally, it probably has implications for the decrease of the self-diffusivity observed for high loadings (Figure 4.11 b) and also contributes to the aggregation of  $N_2$  (Figure. 4.16). To obtain further insights, this work studied also interactions between N-N atoms of  $N_2$  molecules in ZIF-8 framework.

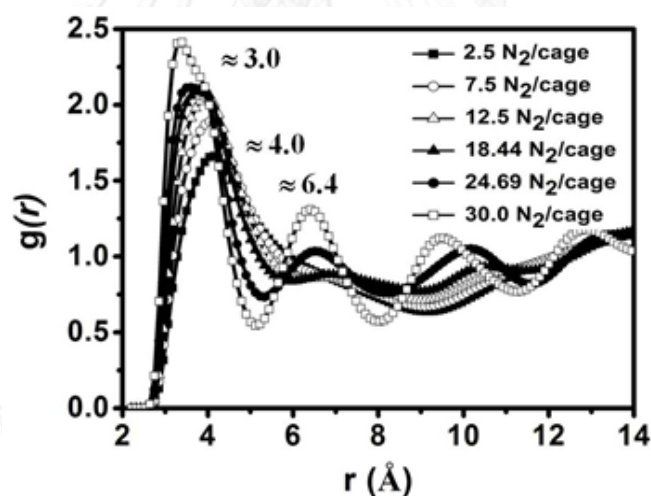


Figure 4.16 RDF between N-N atoms for a  $N_2$  molecule at different loadings in ZIF-8 framework.

At low to intermediate loadings (2.5 to 18.44  $N_2$ /cage) the first peak showed up around 4.0 Å while at high loading (24.69 to 30.0  $N_2$ /cage) the first peak is already found around 3.0 Å and a second peak around 6.4 Å. The intense first peak with a visible shoulder was found only at high  $N_2$  loadings. This indicates that a much closer packing of the  $N_2$  molecules is observed at high loadings, as discussed in the probability density plots section.



A population of the sites near the 4-ring windows is also examined for high  $C_2H_6$  loadings, conversely without a swing-effect of the linkers. As revealed by the work of [34, 36, 83], the occurrence of guest-induced structural transitions in ZIF-8 is the effect of a complex interplay of different factors, with guest size, shape, packing and interaction with the linker molecules and related changes in the energy landscape of the host structure. Hence, most likely, it is not only a consequence of the somewhat larger size of  $C_2H_6$  compared to  $N_2$ , that a gate-opening transition is not observed for  $C_2H_6$ . Nevertheless, the situation might change in other ZIF structures. In [84] by quantum density functional simulations of  $C_2H_6$  in ZIF-7, a quantum mechanical effect for the gate-opening was suggested. This emphasizes to the conclusion that within the highly flexible ZIF lattices a complex interplay of the host-guest system results in gate-opening effects. In case of  $N_2$  in ZIF-8, classical simulations are sufficiently accurate to capture its dynamic occurrence.

A structural transform caused by  $C_2H_6$  uptake was found in classical simulation for another MOF structure, viz. MOF Zn(tbip) [85, 86]. At higher loadings an increase of the diameter of the bottlenecks in the channels occurred that results in a rapid increase of the self-diffusion coefficient. Fascinatingly, this opening of the bottleneck could only be observed for  $C_2H_6$ , not for  $CH_4$ , whereas for ZIF-8 the classical gate-opening appears for  $N_2$ , but not for  $C_2H_6$  [19, 87]. For  $N_2$  in ZIF-8, the increase of the window size is not connected with an increase in the diffusivity (Figure 4.11 b). Actually, the reorientation and closer packing of the  $N_2$  molecules at higher loadings has also implications for their mobility. Besides the size of the narrow window also the probability to jump throughout the window and the opportunity to find a free site behind contribute to the diffusivity. Induced by the structural transition and the rearrangement, the chance to find  $N_2$  in the window region is notably increased. Moreover, the closer packing makes it more difficult for the  $N_2$  molecules to exchange their places. Both contributions overbalance the speed-up in the diffusivity which would be expected exclusively based on the window size and result in decline of the self-diffusivity above 18.4 molecules/ cage (Figure 4.11 b). In conclusion, at 30  $N_2$  molecules/cage the  $N_2$  molecules can swing only in isolated regions (Figure 4.14 f), resulting in the sharp reduction of the mobility.

### 4.3 Quantum chemical calculations

In this part quantum chemical calculations were used to study the information about rotational energy of the linker such a 4- and 6-membered ring in ZIF-8. The total atoms in 4- and 6-membered ring are 140 and 210 atoms, respectively. The energy values for linker orientations in 4- and 6-membered ring can be seen in Figure 4.17.

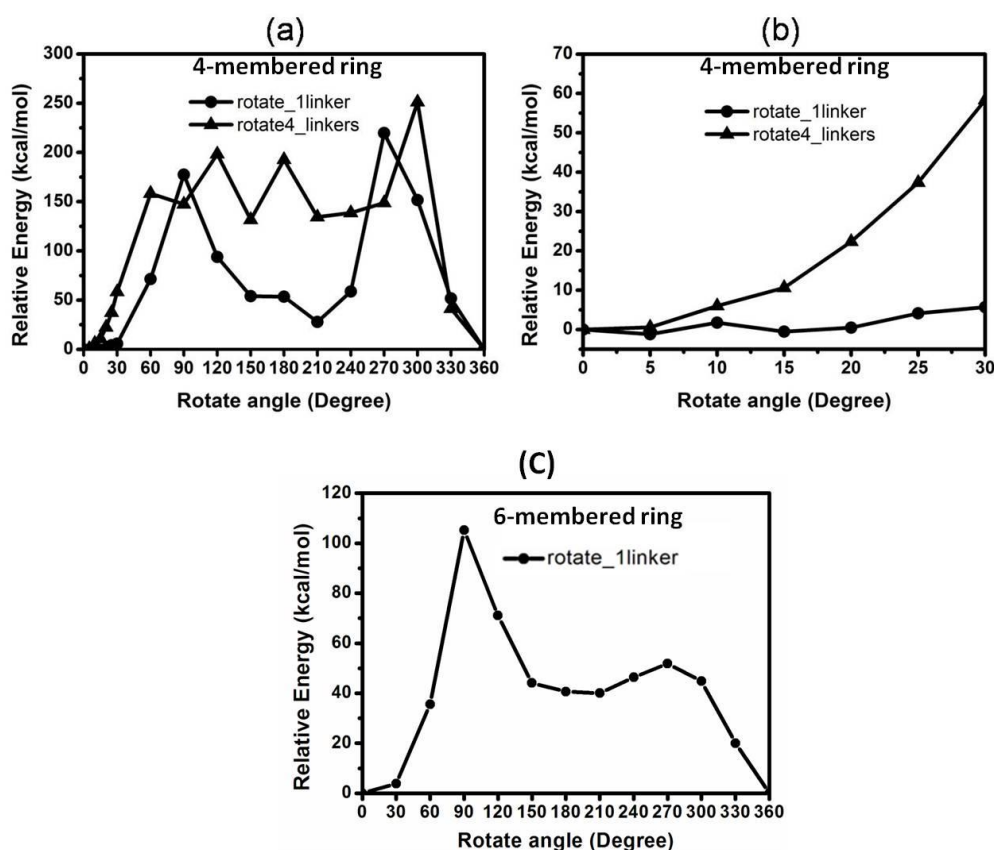


Figure 4.17 The relative energy (kcal/mol) obtained from the quantum chemical calculations for the ZIF-8 linkers turning in the 4-membered ring in the ranges  $0^{\circ}$ - $360^{\circ}$  (a) and  $0^{\circ}$  - $30^{\circ}$  (b), and 6-membered ring in the ranges  $0^{\circ}$  - $360^{\circ}$  (c).

In Figure 4.17 (a) the range of 0-360 degree is tested at every 30 degree and (b) which focus on the energies in the range of 0-30 degree with an interval of 5 degree in 4-membered ring. The energy thresholds for such a process turn out to be such high that rotations on large angles or transitions to another minimum in Figure 4.17 (a) are extremely unlikely. Figure 4.17 (b) can see that the energy necessary to

rotate 4 linkers in the 4-membered ring is approximately 4 times that of the rotation of one linker. Thus, even in the comparably small 4-membered ring the mutual interaction between linkers is negligible. Figure 4.17 (b) also demonstrates that rotation of the linker by about 13 degrees as found in [84] in density functional calculations for ZIF-7 with guest molecules would also be no problem for the ZIF-8 with our parameter set C. The more detailed quantum chemical investigation of the window region (6-membered ring) including the surrounding parts of the lattice was shown in Figure 4.17 (c), with energy thresholds in the range of 0-360 degree. The energy thresholds for rotation of one linker in 6-membered ring were found asymmetric as in 4-membered ring that can be explained in Figure 4.18.

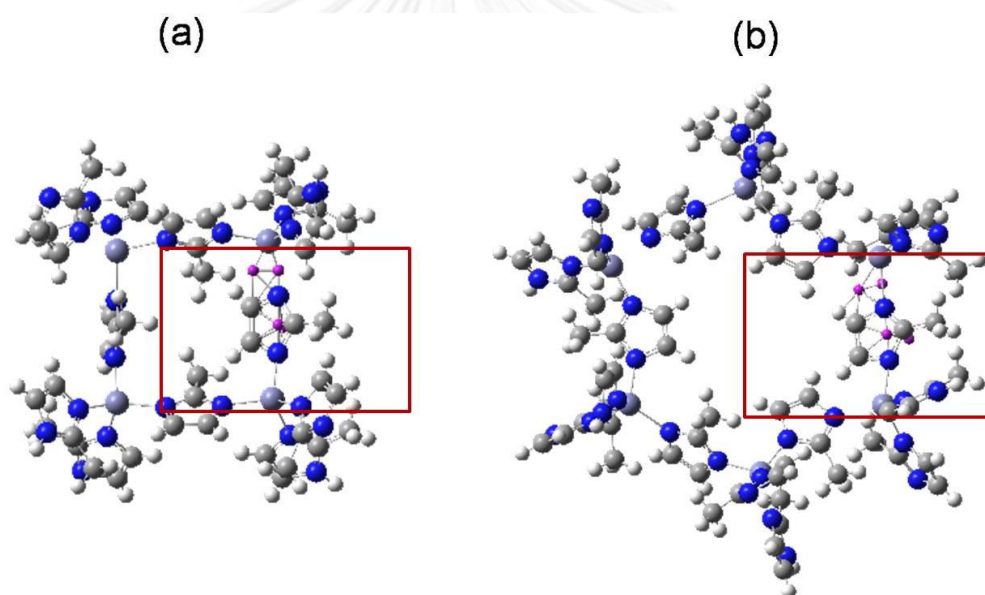


Figure 4.18 (a) Structures of 4-membered ring and (b) 6-membered ring.

Figure 4.18 shows the rotation of one linker in 4- and 6-membered ring at  $90^\circ$  which in this position the energy thresholds were found around 200 and 110 kcal/mol for 4- and 6-membered, respectively. Because the methyl group of the rotating linker has a steric effect with other methyl groups in 4- and 6-membered (outside window) as shown in the red square. When the rotation of one linker was at  $270^\circ$  in both systems then the methyl group of the linker returned inside the window so that energy thresholds were obtained about 200 and 50 kcal/mol for 4- and 6-membered ring, respectively. Since the steric effect from methyl groups was found for 4-membered ring but not for 6-membered ring.

Note that in this examination the remaining parts of the lattice were kept rigid and unchanged. Thus, these results mean that large rotation angles are impossible in this simplified model. Swinging of the linker by more than 30 degrees whereas the remaining parts of the lattice keep unmodified seems to be unlikely from these results. If gate opening to larger rotational angles happens in that case, at least during a period of transition, collective changes in the lattice must be expected. However, this is far from being understood in this calculation because the total ZIF-8 lattice is too large and too complicated for quantum chemical calculations.



## CHAPTER V

### CONCLUSIONS

The flexible lattice is really sensitive with respect to the force constants and partial charges of the lattice atoms. The alternative of parameters from Zheng et al. [35] and Zhang et al. [36] maintain the total size of the simulation box well in NPT simulations. However, these two parameter sets yield deformations of the window size which disagree with the XRD obtained lattice structure. Furthermore, the parameter set [35] does not allow the diffusion of  $C_2H_6$  in disagreement with experiments. This work uses the parameter set from Hertäg et al. [19] slightly modified. A stronger force constant in terms of the Zn-N bond as suggested in [35] improved preservation of the box size in NPT simulations. Then, it has been adjusted to parameter set C as expressed in this work and used to study  $C_2H_6$  and  $N_2$  in flexible ZIF-8 lattice.

The simulation results of  $C_2H_6$  demonstrate the fascinating effect that with increasing loading of  $C_2H_6$  molecules the self-diffusion coefficient is almost unchanged. This is owing to two reasons of dissimilar nature that nearly balance each other. The first reason is of entropic nature: the window diameter becomes smaller with increasing loading, making it more complicated for  $C_2H_6$  molecules to discover the window. Although, simultaneously at higher loadings the  $C_2H_6$  molecules outside the window generate forces that push the probe molecule into the window if the window is not already occupied.

This work also is also focused on studying the impact of structural changes on the dynamics of  $N_2$  molecules in the ZIF-8 by MD simulations. A so called gate-opening effect was mentioned in several articles. There is strong experimental support for the change of the structure of ZIF-8 from closed to open windows. The results of this work for  $N_2$  demonstrate that the parameter set as suggested in [19] for  $C_2H_6$  molecules (parameter set C) can reproduce the guest-induced transform of the ZIF-8 lattice structure by MD simulations performed in the NVE ensemble. The structural change in this simulation is also matching with the structural transition expressed previously in the article by Fairen-Jiminez et al. [34]. Another parameter set developed newly by Zhang et al. [36] is able to keep the unit cell dimensions,  $N_2$  adsorption and mechanical properties in NPT simulations except the correct window diameter. However, the parameter set recommended in [36], for parameter set C is found to yield the diameter of the windows connecting neighboring cavities nearly completely equivalent to results of the X-ray experiments. As the window diameter

is of fundamental importance for the diffusion of molecules with diameters close to the window size, this work supposes that parameter set C may present a more realistic prediction of guest diffusion like  $C_2H_6$  molecules in ZIF-8. In agreement with the experiments, these simulations point to gate-opening at a high concentration of 18.4  $N_2$  molecules/cage. At this critical  $N_2$  loading, the methylimidazolate linkers have to distort to allow the adsorption of additional  $N_2$  molecules. Most interestingly, the evidential increase in the window size by 0.36 Å does not result in a speed-up of the molecular mobility. The accelerating effect of the larger window size appears to be overcompensated by relationship of different factors initiated by the relocation of the  $N_2$  molecules above the “gate-loading”. These results include stronger interactions between the  $N_2$  molecules and the enhanced probability to discover  $N_2$  molecules in the window region. This leads to an increased mutual hindrance which overbalances the expected mobility increase based on the larger window size, and results in the observed decline of the self-diffusivity. The situation might be different for a hypothetical molecule, which induces similar structural changes but, has a size closer to the limiting dimensions of the windows connecting the cavities.

Quantum chemical calculations demonstrate that the energy for rotation of the linker in 4-membered ring for more than 13 degrees that means rotations on large angles is different from rotation of one linker. Moreover, the torsional linker motion in 4- and 6-membered ring demonstrated at least that the sometimes proposed picture of a swinging linker seems to be too simple under conditions of unchanged remaining parts of the lattice. From the literature and our results, it is confirmed that the gate opening is a phenomenon in the presence of guest molecules in which the lattice atoms other than linker atoms also move. The gate opening effect could not be found in our classical MD simulations for  $C_2H_6$  in ZIF-8 but it is explained in ZIF-7 system [84] that this relates to quantum effects.

## REFERENCES

1. Ackley, M.W., S.U. Rege, and H. Saxena, *Application of natural zeolites in the purification and separation of gases*. Microporous and Mesoporous Materials, 2003. **61**(1–3): p. 25-42.
2. Bowen, T.C., R.D. Noble, and J.L. Falconer, *Fundamentals and applications of pervaporation through zeolite membranes*. Journal of Membrane Science, 2004. **245**(1–2): p. 1-33.
3. Czaja, A.U., N. Trukhan, and U. Muller, *Industrial applications of metal-organic frameworks*. Chemical Society Reviews, 2009. **38**(5): p. 1284-1293.
4. Mueller, U., et al., *Metal-organic frameworks-prospective industrial applications*. Journal of Materials Chemistry, 2006. **16**(7): p. 626-636.
5. Wight, A.P. and M.E. Davis, *Design and Preparation of Organic-Inorganic Hybrid Catalysts*. Chemical Reviews, 2002. **102**(10): p. 3589-3614.
6. Yamamoto, K., et al., *Organic-Inorganic Hybrid Zeolites Containing Organic Frameworks*. Science, 2003. **300**(5618): p. 470-472.
7. Yaghi, O.M., et al., *Reticular synthesis and the design of new materials*. Nature, 2003. **423**: p. 705-714
8. Park, K.S., et al., *Exceptional chemical and thermal stability of zeolitic imidazolate frameworks*. Proceedings of the National Academy of Sciences, 2006. **103**(27): p. 10186-10191.
9. Hayashi, H., et al., *Zeolite A imidazolate frameworks*. Nature Materials, 2007. **6**: p. 501 - 506
10. Wang, B., et al., *Colossal cages in zeolitic imidazolate frameworks as selective carbon dioxide reservoirs*. Nature, 2008. **453**: p. 207-211.
11. Liu, B. and B. Smit, *Molecular Simulation Studies of Separation of CO<sub>2</sub>/N<sub>2</sub>, CO<sub>2</sub>/CH<sub>4</sub>, and CH<sub>4</sub>/N<sub>2</sub> by ZIFs*. The Journal of Physical Chemistry C, 2010. **114**(18): p. 8515-8522.
12. Reyes, S.C., et al., *Separation of methane from higher carbon number hydrocarbons utilizing zeolitic imidazolate framework materials*. 2009, Google Patents.
13. Bux, H., et al., *Zeolitic Imidazolate Framework Membrane with Molecular Sieving Properties by Microwave-Assisted Solvothermal Synthesis*. Journal of the American Chemical Society, 2009. **131**(44): p. 16000-16001.
14. Bux, H., et al., *Novel MOF-Membrane for Molecular Sieving Predicted by IR-Diffusion Studies and Molecular Modeling*. 2010. **22**: p. 4741-4743.

15. Luebbers, M.T., et al., *Effects of Molecular Sieving and Electrostatic Enhancement in the Adsorption of Organic Compounds on the Zeolitic Imidazolate Framework ZIF-8*. *Langmuir*, 2010. **26**(19): p. 15625-15633.
16. Li, K., et al., *Zeolitic Imidazolate Frameworks for Kinetic Separation of Propane and Propene*. *Journal of the American Chemical Society*, 2009. **131**(30): p. 10368-10369.
17. Peralta, D., et al., *Comparison of the Behavior of Metal–Organic Frameworks and Zeolites for Hydrocarbon Separations*. *Journal of the American Chemical Society*, 2012. **134**(19): p. 8115-8126.
18. Zhang, C., et al., *Unexpected Molecular Sieving Properties of Zeolitic Imidazolate Framework-8*. *The Journal of Physical Chemistry Letters*, 2012. **3**(16): p. 2130-2134.
19. Hertäg, L., et al., *Diffusion of CH<sub>4</sub> and H<sub>2</sub> in ZIF-8*. *Journal of Membrane Science*, 2011. **377**(1–2): p. 36-41.
20. Pantatosaki, E., et al., *On the Impact of Sorbent Mobility on the Sorbed Phase Equilibria and Dynamics: A Study of Methane and Carbon Dioxide within the Zeolite Imidazolate Framework-8*. *The Journal of Physical Chemistry C*, 2011. **116**(1): p. 201-207.
21. Haldoupis, E., S. Nair, and D.S. Sholl, *Efficient Calculation of Diffusion Limitations in Metal Organic Framework Materials: A Tool for Identifying Materials for Kinetic Separations*. *Journal of the American Chemical Society*, 2010. **132**(21): p. 7528-7539.
22. Thornton, A.W., et al., *Feasibility of zeolitic imidazolate framework membranes for clean energy applications*. *Energy & Environmental Science*, 2012. **5**(6): p. 7637-7646.
23. Banerjee, R., et al., *High-Throughput Synthesis of Zeolitic Imidazolate Frameworks and Application to CO<sub>2</sub> Capture*. *Science*, 2008. **319**(5865): p. 939-943.
24. Xu, R., et al., *Chemistry of Zeolites and Related Porous Materials: Synthesis and Structure*. 2007, Singapore: John Wiley & Sons (Asia) Pte Ltd.
25. Huang, A., et al., *Molecular-Sieve Membrane with Hydrogen Permselectivity: ZIF-22 in LTA Topology Prepared with 3-Aminopropyltriethoxysilane as Covalent Linker*. 2010. **49**: p. 4958–4961.
26. Liu, Y., et al., *Synthesis and characterization of ZIF-69 membranes and separation for CO<sub>2</sub>/CO mixture*. *Journal of Membrane Science*, 2010. **353**(1–2): p. 36-40.
27. Zakzeski, J., et al., *Catalytic oxidation of aromatic oxygenates by the heterogeneous catalyst Co-ZIF-9*. *Applied Catalysis A: General*, 2011. **394**(1–2): p. 79-85.
28. Nguyen, L.T.L., et al., *Metal-organic frameworks for catalysis: the Knoevenagel reaction using zeolite imidazolate framework ZIF-9 as an efficient heterogeneous catalyst*. *Catalysis Science & Technology*, 2012. **2**(3): p. 521-528.



29. Nguyen, L.T.L., K.K.A. Le, and N.T.S. Phan, *A Zeolite Imidazolate Framework ZIF-8 Catalyst for Friedel-Crafts Acylation*. Chinese Journal of Catalysis, 2012. **33**(4–6): p. 688-696.
30. Sun, C.-Y., et al., *Zeolitic imidazolate framework-8 as efficient pH-sensitive drug delivery vehicle*. Dalton Transactions, 2012. **41**(23): p. 6906-6909.
31. Zhou, M., et al., *Adsorption Sites of Hydrogen in Zeolitic Imidazolate Frameworks*. The Journal of Physical Chemistry B, 2009. **113**(32): p. 11049-11053.
32. Moggach, S.A., T.D. Bennett, and A.K. Cheetham, *The Effect of Pressure on ZIF-8: Increasing Pore Size with Pressure and the Formation of a High-Pressure Phase at 1.47 GPa*. 2009. **48**: p. 7087-7089.
33. Assfour, B., S. Leoni, and G. Seifert, *Hydrogen Adsorption Sites in Zeolite Imidazolate Frameworks ZIF-8 and ZIF-11*. The Journal of Physical Chemistry C, 2010. **114**(31): p. 13381-13384.
34. Fairen-Jimenez, D., et al., *Opening the Gate: Framework Flexibility in ZIF-8 Explored by Experiments and Simulations*. Journal of the American Chemical Society, 2011. **133**(23): p. 8900-8902.
35. Zheng, B., et al., *Force Field for Molecular Dynamics Computations in Flexible ZIF-8 Framework*. The Journal of Physical Chemistry C, 2011. **116**(1): p. 933-938.
36. Zhang, L., Z. Hu, and J. Jiang, *Sorption-Induced Structural Transition of Zeolitic Imidazolate Framework-8: A Hybrid Molecular Simulation Study*. J. Am. Chem. Soc., 2013. **135**(9): p. 3722–3728.
37. Leach, A.R., *Molecular modeling: Principles and applications*. 2 ed. 2001, England: Pearson Education Limited.
38. Lewars, E.G., *Computational chemistry: Introduction to the theory and applications of molecular and quantum mechanics*. 2003, Dordrecht: Kluwer Academic Publishers.
39. Haile, J.M., *Molecular Dynamics Simulation: Elementary Methods*. 1992, New York: John Wiley & Sons, Inc.
40. Cohen, I.B., *Revolution in science*. 1985, Cambridge: Harvard University Press.
41. Allen, M.P. and D.J. Tildesley, *Computer Simulation of Liquids*. 1989, Oxford University Press: New York.
42. Rapaport, D.C., *The Art of Molecular Dynamics Simulation*. 2004, New York: Cambridge University Press.
43. Beeman, D., *Some multistep methods for use in molecular dynamics calculations*. Journal of Computational Physics, 1976. **20**(2): p. 130-139.

44. Swope, W.C., et al., *A computer simulation method for the calculation of equilibrium constants for the formation of physical clusters of molecules: Application to small water clusters*. 1982. **76**(1): p. 637-649.
45. Jensen, F., *Introduction to computational chemistry*. 2 ed. 2007, England: John Wiley & Sons Ltd.
46. Santen, R.A.v. and P. Sautet, *Computational methods in catalysis and materials science: An introduction for scientists and engineers*. 2009, Weinheim: Wiley-VCH.
47. Hinchliffe, A., *Molecular modelling for beginners*. 2 ed. 2008, United Kingdom: John Wiley & Sons Ltd.
48. Jost, W., *Diffusion in solids, liquids and gases*. 1960, New York: Academic Press.
49. Schuring, D., *Diffusion in zeolites: Towards a microscopic understanding*, in *Catalyst*. 2002, Eindhoven University of Technology: Netherlands.
50. Fick, A., *Ueber diffusion*. Pogg. Ann. Phys. Chem., 1855. **170**: p. 59-86.
51. Barrer, R.M. and W. Jost, *A note on interstitial diffusion*. Transactions of the Faraday Society, 1949. **45**(0): p. 928-930.
52. Einstein, A., *On the movement of small particles suspended in stationary liquids required by the molecular-kinetic theory of heat*. Ann. Phys. , 1905. **17**: p. 549-560.
53. Kärger, J. and D.M. Ruthven, *Diffusion in zeolites and other microporous solids*. 1992, New York: John Wiley & Sons, Inc.
54. Kärger, J., H. Pfeifer, and W. Heink, *Principles and applications of self-diffusion measurements by nuclear magnetic resonance* Adv. Magn. Res., 1988. **12**: p. 1-89.
55. Theodorou, D.N., R.Q. Snurr, and A.T. Bell, *Molecular dynamics and diffusion in microporous materials*. 1996, Oxford: Pergamon Press.
56. Hehre, W.J., *A guide to molecular mechanics and quantum chemical calculations*. 2003, United States of America: Wavafunction, Inc.
57. Akins, P.W. and R.S. Friedman, *Molecular quantum mechanics*. 3 ed. 1997, New York: Oxford University Press.
58. Schrödinger, E., *Quantisierung als Eigenwertproblem*. Ann. Phys., 1926. **79**: p. 361-376.
59. Schrödinger, E., *An undulatory theory of the mechanics of atoms and molecules*. Phys. Rev., 1926. **28**: p. 1049-1070.
60. Szabo, A. and N.S. Ostlund, *Modern quantum chemistry: Introduction to advanced electronic structure theory*. 1989, USA: Mcgraw-Hill.
61. Levin, I.N., *Quantum chemistry*. 5 ed. 2000, University of New York: Prentice Hall.
62. Cramer, C.J., *Essentials of computational chemistry: Theories and models*. 2 ed. 2004, England: John Wiley & Sons Ltd.

63. Parr, R.G. and Y. Weitao, *Density-functional theory of atoms and molecules*. 1989, New York: Oxford University Press.
64. Lee, C., W. Yang, and R.G. Parr, *Development of the Colle-Salvetti correlation energy formula into a functional of the electron density*. *Phys. Rev. B*, 1988. **37**(2): p. 785-789.
65. Becke, A.D., *Density-functional thermochemistry. III. The role of exact exchange*. *J. Chem. Phys.*, 1993. **98**: p. 5648-5652.
66. Kahn, L.R., P. Baybutt, and D.G. Truhlar, *Ab initio effective core potentials: Reduction of all-electron molecular structure calculations to calculations involving only valence electrons*. *J. Chem. Phys.*, 1976. **65**: p. 3826-3863.
67. J.Hay, P. and W.R. Wadt, *Ab initio effective core potentials for molecular calculations: Potentials for the transition metal atoms Sc to Hg*. *J. Chem. Phys.*, 1985. **82**: p. 270-283.
68. CSAR, *DL\_POLY*. 2006, High Performance Computing service: UK.
69. Martin, M. and J. Siepmann, *Transferable Potentials for Phase Equilibria. 1. United-Atom Description of n-Alkanes*. *J. Phys. Chem. B*, 1998. **102**(14): p. 2569-2577.
70. Potoff, J.J. and J.I. Siepmann, *Vapor-liquid equilibria of mixtures containing alkanes, carbon dioxide, and nitrogen*. *AIChE Journal*, 2001. **47**(7): p. 1676-1682.
71. Bux, H., et al., *Ethene/ethane separation by the MOF membrane ZIF-8: Molecular correlation of permeation, adsorption, diffusion*. *Journal of Membrane Science*, 2011. **369**(1-2): p. 284-289.
72. Chmelik, C., et al., *Ethene/ethane mixture diffusion in the MOF sieve ZIF-8 studied by MAS PFG NMR diffusometry*. *Microporous and Mesoporous Materials*, 2012. **147**(1): p. 135-141.
73. Frisch, M.J., G.W. Trucks, and H.B. Schlegel, *Gaussian 03*. 2004, Gaussian, Inc.: Wallingford, Conn, USA
74. Babarao, R., S. Dai, and D.-e. Jiang, *Effect of Pore Topology and Accessibility on Gas Adsorption Capacity in Zeolitic-Imidazolate Frameworks: Bringing Molecular Simulation Close to Experiment*. *The Journal of Physical Chemistry C*, 2011. **115**(16): p. 8126-8135.
75. Chandler, D., *Statistical mechanics of isomerization dynamics in liquids and the transition state approximation*. *The Journal of Chemical Physics*, 1978. **68**(6): p. 2959-2970.
76. Chandler, D., *Introduction to Modern Statistical Mechanics*. 1987, New York: Oxford University Press.
77. Pusch, A.-K., et al., *NMR studies of carbon dioxide and methane self-diffusion in ZIF-8 at elevated gas pressures*. *Adsorption*, 2012. **18**(5-6): p. 359-366.

78. Battisti, A., S. Taioli, and G. Garberoglio, *Zeolitic imidazolate frameworks for separation of binary mixtures of CO<sub>2</sub>, CH<sub>4</sub>, N<sub>2</sub> and H<sub>2</sub>: A computer simulation investigation*. Microporous and Mesoporous Materials, 2011. **143**(1): p. 46-53.
79. E, P., et al., *Probing the hydrogen equilibrium and kinetics in zeolite imidazolate frameworks via molecular dynamics and quasi-elastic neutron scattering experiments*. 2013. **138**(3): p. 034706.
80. Haldoupis, E., et al., *Quantifying Large Effects of Framework Flexibility on Diffusion in MOFs: CH<sub>4</sub> and CO<sub>2</sub> in ZIF-8*. ChemPhysChem, 2012. **13**(15): p. 3449-3452.
81. Kitagawa, S. and K. Uemura, *Dynamic porous properties of coordination polymers inspired by hydrogen bonds*. Chemical Society Reviews, 2005. **34**(2): p. 109-119.
82. Wu, H., W. Zhou, and T. Yildirim, *Hydrogen Storage in a Prototypical Zeolitic Imidazolate Framework-8*. Journal of the American Chemical Society, 2007. **129**(17): p. 5314-5315.
83. Ania, C.O., et al., *Understanding Gas-Induced Structural Deformation of ZIF-8*. The Journal of Physical Chemistry Letters, 2012. **3**(9): p. 1159-1164.
84. van den Bergh, J., et al., *Understanding the Anomalous Alkane Selectivity of ZIF-7 in the Separation of Light Alkane/Alkene Mixtures*. Chemistry – A European Journal, 2011. **17**(32): p. 8832-8840.
85. Seehamart, K., et al., *A Molecular Dynamics investigation of the influence of framework flexibility on self-diffusivity of ethane in Zn(tbip) frameworks*. Microporous and Mesoporous Materials, 2009. **125**(1-2): p. 97-100.
86. Seehamart, K., et al., *Investigating the reasons for the significant influence of lattice flexibility on self-diffusivity of ethane in Zn(tbip)*. Microporous and Mesoporous Materials, 2010. **130**(1-3): p. 92-96.
87. Chokbunpiam, T., et al., *The importance of lattice flexibility for the migration of ethane in ZIF-8: Molecular dynamics simulations*. Microporous and Mesoporous Materials, 2013. **174**(0): p. 126-134.
88. Reimann, S., *Studies of the lattice dynamics of the metal-organic framework ZIF-8, in Physics*. 2011, University of Leipzig: Leipzig.
89. Becker, F.-M., et al., *Formeln und Tabellen für die Sekundarstufen I und II*. 2008, Berlin: Duden Paetec Schulbuchverlag.



APPENDIX

จุฬาลงกรณ์มหาวิทยาลัย  
**CHULALONGKORN UNIVERSITY**

## APPENDIX A

Interaction parameters for the flexible models of ZIF-8 framework,  $C_2H_6$ ,  $N_2$  and the procedure of evaluating the window diameter.



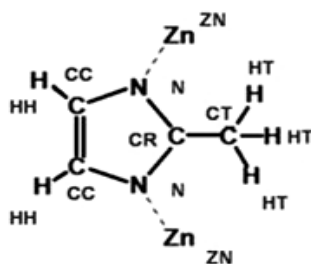


Figure A.1 Atom types in the rotating linker of ZIF-8.

### 1. Bond force constant

The parameters for bond, bending angle and torsion angle employed in this work, if not clearly mentioned, are the similar with Hertäg et al. [19]. Examining lattice size effects among the interactions for example bond, bending angle, dihedral torsion angle and electrostatic interaction deserve particular attention. Thus, bond lengths  $r$  (Å) and force constants  $k_r$  (kcal/mol/Å<sup>2</sup>) from Hertäg et al. [19], Zheng et al [35] and Zhang et al. [36] have to be evaluated. The bond potential is modeled by a harmonic oscillation potential.

$$U_{bond} = \sum \frac{1}{2} k_r (r_{ij} - r_0)^2 \quad (1)$$

By  $U_{bond}$ ,  $r_{ij}$ , and  $r_0$  refer to potential energy, distance and equilibrium value of the distance, respectively. Note that in [35] the division by 2 in formula (35) is absent and then the  $k_r$  are smaller approximately by the factor of 1/2 (see Table A.1). Table A.1 presents the constants for bonds between dissimilar kinds of lattice atoms.

**Table A.1** Overview over the bond lengths (Å) and force constants (kcal/mol/Å<sup>2</sup>) of ZIF-8 from Hertäg et al. [19], Zheng et al [35] and Zhang et al. [36] are applied in this work. For the classification of atom types *i* and *j* notice in Figure A.1.

Atom type		From [19]		From [35]		From [36]	
<i>i</i>	<i>J</i>	$k_r$	$r_0$	$k_r$	$r_0$	$k_r$	$r_0$
CC	CC	1036	1.371	540.249	1.350	1036	1.346
CC	N	820	1.385	440.210	1.370	820	1.371
CC	HH	734	1.080	367.000	1.080	734	0.929
CT	HT	680	1.090	340.000	1.090	680	0.959
CR	N	996	1.335	488.000	1.335	976	1.339
ZN	N	40	2.050	78.500	2.011	172	1.987
CR	CT	634	1.504	346.543	1.490	634	1.492

Mainly, the bond lengths ( $r_0$ ) and force constants ( $k_r$ ) from [19], [35] and [36] for the dissimilar kinds of bonds are only slightly different (taking into account the factor 0.5 as mentioned in [19] and [36]). Only the Zn-N bond, is significantly different. Whereas this force constant  $k_r$  has a value of 40 kcal/mol/Å<sup>2</sup> in [19] its value in [35] is 78.5 kcal/mol/Å<sup>2</sup> and under consideration of the factor of 2 in equation 1. It is 157 kcal/mol/Å<sup>2</sup>. For Zn-N bond in [36] also have larger values of this force constant  $k_r$  than [19] its value in is 172 kcal/mol/Å<sup>2</sup> when using the same equation 1 with [19]. (Table A.1). The parameters from [19] and [35] will be compared in this work.

## 2. Bending force constant

The bending angle, that is a three body effect between given atoms *i*, *j* and *k* is up to second order of the deviation of the angle  $\theta_{ijk}$  from its equilibrium value  $\theta_0$  explained by this equation.

$$U_{\text{angle}}(\theta_{ijk}) = \sum \frac{1}{2} k_{\theta} (\theta_{ijk} - \theta_0)^2 \quad (2)$$

The bending angle ( $\theta_0$ ) and bending angle force constants ( $k_{\theta}$ ) from [19], [35] and [36], are significantly dissimilar taking into account the factor of 2 as explicated



before. While the force constants  $k_{\theta}$  for CC-N-Zn, CR-N-Zn and N-Zn-N have the value of 20 kcal/mol/deg<sup>2</sup> in [19], greatly larger values of this force constant  $k_{\theta}$  are reported in [35] and amount 32.477, 48.68 and 35.24 kcal/mol/deg<sup>2</sup>, correspondingly. In consideration of the absenting factor 2, these  $k_{\theta}$  data amount according to equation 2 with 64.954, 97.36 and 70.48 kcal/mol/deg<sup>2</sup>. For CC-N-Zn and CR-N-Zn in [36] also have larger values of this force constant  $k_{\theta}$  with 70 and 100 kcal/mol/deg<sup>2</sup> than [19] when using the same equation 2 (Table A.2).

**Table A.2** Overview over the equilibrium bending angle  $\theta_0$  (deg) and force constants  $k_{\theta}$  (kcal/mol/deg<sup>2</sup>) of ZIF-8, taken from from Hertäg et al. [19], Zheng et al. [35] and Zhang et al. [36] applied in this work. For the classification of the atom types  $i$ ,  $j$ , and  $k$ , notice in Figure A.1.

Atom type			From [19]		From [35]		From [36]	
$i$	$j$	$K$	$k_{\theta}$	$\theta_0$	$k_{\theta}$	$\theta_0$	$k_{\theta}$	$\theta_0$
CC	CC	N	140	120	73.75	108.65	140	108.67
CC	CC	HH	100	120	49.451	125.67	100	125.67
CR	CT	HT	100	109.5	48.088	109.32	100	109.44
HT	CT	HT	70	109.5	35	109.5	70	109.50
CC	N	ZN	20	126	32.477	126.40	70	128.0
CR	N	ZN	20	126	48.68	128.32	100	127.50
CC	N	CR	140	120	71.254	105.27	140	105.24
N	ZN	N	20	109.5	35.24	126.40	21	109.47
N	CR	N	140	120	75.484	112.16	140	112.17
N	CR	CT	140	120	66.051	123.89	140	123.89
N	CC	HH	140	120	49.954	125.68	100	125.66

### 3. Torsion force constant

The torsional also called dihedral interaction that is a 4 body effect of 4 atoms  $i,j,k,l$  is modeled by this equation.

$$U_{torsion}(\phi_{ijkl}) = \sum k_{\phi}[1 + \cos(n\phi_{ijkl} - \phi_0)] \quad (3)$$

By  $U_{torsion}$ ,  $k_{\phi}$  and  $\phi_0$  representing the potential energy, force constant, torsional angle and equilibrium value of the torsional angle, respectively.

**Table A.3** Overview over the equilibrium torsional angles  $\phi_0$  (deg) and torsion force constants  $k_{\phi}$  (kcal/mol) of ZIF-8, that were taken from Hertäg et al. [19] and Zheng et al. [35] are applied in this work. For the classification of the atom types  $i, j, k$  and  $l$ , notice in Figure A.1.

Atom type				From [19]			From [35]		
$i$	$j$	$K$	$l$	$k_{\phi}$	$\phi_0$	n	$k_{\phi}$	$\phi_0$	n
X	N	CC	X	6	180	2	2.324	180	2
X	CC	CC	X	21.5	180	2	5.150	180	2
X	CR	N	X	10	180	2	5.00	180	2

For the torsional interaction from Zhang et al. [36] is spited into two parts such as proper and improper as shown in equation 4 and 5, respectively.

$$U_{proper}(\phi_{ijkl}) = \sum k_{proper}[1 + \cos(n\phi_{ijkl} - \phi_0)] \quad (4)$$

$$U_{improper}(\phi_{ijkl}) = \sum k_{improper}[1 + \cos(n\phi_{ijkl} - \phi_0)] \quad (5)$$

**Table A.4** Overview over the equilibrium torsional angles  $\phi_0$  (deg) and torsion force constants  $k_{\text{proper}}$  (kcal/mol) of ZIF-8, which were taken from Zhang et al. [36]). For the classification of the atom types  $i, j, k$  and  $l$ , notice in Figure A.1.

Atom type				From [36]		
$i$	$j$	$K$	$l$	$k_{\text{proper}}$	$\phi_0$	$n$
CC	N	CR	N	4.8	180	2
CC	N	CR	CT	4.15	180	2
CR	N	CC	CC	4.8	180	2
CR	N	CC	HH	4.8	180	2
N	CC	CC	N	4	180	2
N	CC	CC	HH	4	180	2
HH	CC	CC	HH	4	180	2
Zn	N	CR	N	0.1	180	2
Zn	N	CR	CT	0.1	180	2
Zn	N	CC	CC	0.1	180	2
N	Zn	N	CR	0.174	0	3
N	Zn	N	CC	0.174	0	3

**Table A.5** Overview over the equilibrium torsional angles  $\phi_0$  (deg) and torsion force constants  $k_{\text{improper}}$  (kcal/mol) of ZIF-8, which were taken from Zhang et al. [36]). For the classification of the atom types  $i, j, k$  and  $l$ , notice in Figure A.1.

Atom type				From [36]		
$i$	$j$	$K$	$l$	$k_{\text{improper}}$	$\phi_0$	$n$
CT	N	CR	N	1.10	180	2
CC	HH	CC	CT	1.10	180	2

#### 4. Atomic partial charge for ZIF-8 framework

**Table A.6** Framework charges from Hertäg et al. [19], Zheng et al. [35] and Zhang et al. [36]. The number of atoms is the number contained in the MD simulation box (8 unit cells). For the classification of the atom types notice Figure A.1.

Atom	Num. of atoms	Charge from [19]	Charge from [35]	Charge from [36]
CC	384	-0.104	-0.1924	-0.1910
CR	192	+0.822	+0.4339	+0.4184
CT	192	-0.585	-0.6024	-0.5726
HH	384	+0.079	+0.1585	+0.1536
HT	576	+0.105	+0.1572	+0.1481
N	384	-0.751	-0.3008	-0.2800
ZN	96	+2.00	+0.7362	+0.6894

The total charge of the lattice from [19] and [36] are zero in order to avoid stability problems throughout the simulations and problems with the Ewald summation. Small adjustments in the parameters below the accuracy of their evaluation from quantum mechanics are sufficient to obtain vanishing total charge. The total lattice charge of [35] is +0.3456. Taking into account that this is the sum of the charges of 2208 lattice atoms in ZIF-8 this non disappearing total charge is very small however, important for procedural reasons.

## 5. Lennard-Jones potential parameters for ZIF-8 framework

**Table A.7** Lennard-Jones (LJ) potential parameters for ZIF-8 framework from Hertäg et al. [19], Zheng et al. [35] and Zhang et al. [36].

Atom	From [19]		From [35]		From [36]	
	L	J	L	J	L	J
CC	0.0860	3.400	0.0860	3.400	0.0567	3.431
CR	0.0860	3.400	0.0860	3.400	0.0567	3.431
CT	0.1094	3.400	0.1094	3.400	0.0567	3.431
HH	0.0150	2.511	0.0150	2.511	0.0238	2.571
HT	0.0157	2.650	0.0157	2.650	0.0238	2.571
N	0.1700	3.250	0.1700	3.250	0.0373	3.261
ZN	0.0125	1.960	0.0125	1.960	0.0670	2.462

## 6. Lennard-Jones potential parameters for C<sub>2</sub>H<sub>6</sub> and N<sub>2</sub>

**Table A.8** Lennard-Jones (LJ) potential parameters and atomic charges for C<sub>2</sub>H<sub>6</sub> and N<sub>2</sub> from Martin et al. [69] and Potoff et al., respectively [70].

Sorbate	Atom	$\sigma(\text{Å})$	$\epsilon/k_b[\text{K}]$	$q(e)$
C <sub>2</sub> H <sub>6</sub>	C	3.73	148.0	0.0
	H	2.50	48.0	0.0
N <sub>2</sub>	N	3.31	36.0	-0.482
	center	0.0	0.0	+0.964

## 7. The procedure of evaluating the window diameter

In this work the aperture diameter is described by calculating the diameter of the largest sphere that is capable to pass the window. In the following, a featured description of the method advised in [88] will be given. As the hydrogen atoms around the window usually do not appearance a circle a special method is required to find this largest sphere. A circle is exclusively described by three points nevertheless there are six hydrogen atoms per pore aperture in ZIF-8 that can limit the size of a sphere that can pass the window.

In the advised method one takes two arbitrary neighboring hydrogen atoms, which are understood to be two positions of a circle (called P1 and P2 in the following). All remaining four atoms are consecutively tried as third position P3 which is needed to describe an absolute circle. The smallest one of these circles communicates to the cross section of the largest sphere that can pass devoid of overlap to one of the hydrogen around the window.

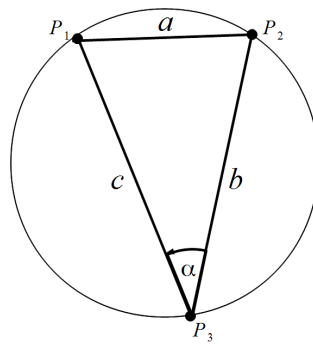


**Figure A.2** The triangle used to describe the window diameter.

Figure A.2 explains the three positions and the triangle that they define as well as the circumcircle. For its radius, the following in this equation holds [89].

$$r = \frac{a}{2\sin\alpha} \quad (6)$$

To find the angle, the law of cosine  $a^2 = b^2 + c^2 - 2bc \cos\alpha$  is employed.

$$r = \frac{a}{2} \left( \frac{b^2 + c^2 - a^2}{2bc} \right)^{-1/2} \quad (7)$$

This method is repeated for all possible neighboring positions P1 and P2, and at the end the choice of P1 and P2 that allows the largest sphere to pass is applied, to identify the window diameter.

## APPENDIX B

The self-diffusion coefficients for  $C_2H_6$  and  $N_2$  in ZIF-8 framework.



**Table B.1** Self-diffusion coefficients of  $C_2H_6$  gases obtained by molecular dynamics simulations with experimental values of the self-diffusion coefficients calculated from transport diffusion IRM data.

Molecule Per cage	Experimental Data		MD simulation by MSD Fitting	
	IRM, sing comp.	MAS PFG NMR, Mixture	Parameter Set A	Parameter Set C
0.05369	$1.06702 \times 10^{-11}$			
0.17744	$1.33155 \times 10^{-11}$			
0.38899	$1.01545 \times 10^{-11}$			
0.5			$5.535 \times 10^{-11}$	$6.48 \times 10^{-11}$
0.84353	$1.0632 \times 10^{-11}$			
1.43091	$9.41767 \times 10^{-12}$			
2.24204	$1.01259 \times 10^{-11}$			
2.5			$6.035 \times 10^{-11}$	$5.85 \times 10^{-11}$
3.21973	$8.27443 \times 10^{-12}$			
3.93031	$6.89941 \times 10^{-12}$	$1.4 \times 10^{-11}$		
4.55	$6.53929 \times 10^{-12}$			
5.0			$6.088 \times 10^{-11}$	$6.23 \times 10^{-11}$
5.15	$7.28583 \times 10^{-12}$			
5.6	$8.92634 \times 10^{-12}$			
5.975	$1.1328 \times 10^{-11}$			
6.325	$1.55368 \times 10^{-11}$			
6.65	$1.70438 \times 10^{-11}$			
7.5			$6.247 \times 10^{-11}$	$6.47 \times 10^{-11}$
8.0		$2.0 \times 10^{-11}$		
10.0			$6.676 \times 10^{-11}$	$6.77 \times 10^{-11}$
12.5			$6.377 \times 10^{-11}$	$6.52 \times 10^{-11}$
15.0			$6.598 \times 10^{-11}$	$6.8 \times 10^{-11}$



**Table B.2** Self-diffusion coefficients from Parameter set C and F of N<sub>2</sub> gases in ZIF-8 obtained by molecular dynamics simulations.

Molecule Per cage	MD simulation by MSD	
	Fitting	
	Parameter Set C	Parameter Set F
0.5	$4.28 \times 10^{-10}$	$4.68 \times 10^{-10}$
2.5	$4.57 \times 10^{-10}$	$3.06 \times 10^{-10}$
5.0	$4.48 \times 10^{-10}$	$7.21 \times 10^{-10}$
7.5	$4.97 \times 10^{-10}$	
10.0	$4.37 \times 10^{-10}$	
12.5	$5.08 \times 10^{-10}$	
15.0	$7.14 \times 10^{-10}$	
17.5	$1.031 \times 10^{-9}$	
18.44	$1.22 \times 10^{-9}$	$1.44 \times 10^{-9}$
20.0	$1.46 \times 10^{-9}$	
22.5	$8.07 \times 10^{-10}$	
24.69	$3.53 \times 10^{-10}$	$8.13 \times 10^{-10}$
25.0	$2.98 \times 10^{-10}$	$7.52 \times 10^{-10}$
27.5	$6.41 \times 10^{-11}$	
30.0	$6.24 \times 10^{-12}$	$3.65 \times 10^{-11}$

## VITA

NAME: Tatiya Chokbunpiam

DATE AND PLACE OF BIRTH: 3 April 1984 in Bangkok, Thailand

EDUCATION:

2003-2007 B. Sc. in General Science, Department of Chemistry, Faculty of Liberal Arts and Science, Kasetsart University, Kamphaeng Saen Campus

2007-2009 M. Sc. in Petrochemistry and Polymer Science, Faculty of Science, Chulalongkorn University, Bangkok

2009-2014 Ph.D. in Petrochemistry, Faculty of Science, Chulalongkorn University, Bangkok

SCHOLARSHIP:

2007-2009 Center of Excellence for Petroleum, Petrochemicals, and Advanced Materials Chulalongkorn University

2007-2009 MRG-WII collaboration with the 90th anniversary of Chulalongkorn University fund (Ratchadaphiseksomphot Endowment Fund) from the Thailand Research Fund

2009-2013 Commission on Higher Education for Sandwich Ph.D. Program (CHE-PHD-SW)

2013-present Ratchadaphiseksomphot Endowment Fund of Chulalongkorn University

PUBLICATIONS:

1. T. Chokbunpiam, P. Thamyongkit, O. Saengsawang, and S. Hannongbua "Molecular Structure and Electronic Properties of Porphyrin-Thiophene-Perylene using Quantum Chemical Calculation" International Journal of Photoenergy. 2010 (2010) 1-9.

2. T. Chokbunpiam, R. Chanajaree, O. Saengsawang, S. Reimann, C. Chmelik, S. Fritzsche, J. Caro, T. Remsungnen and S. Hannongbua "The Importance of Lattice Flexibility for the Migration of Ethane in ZIF-8: Molecular Dynamics Simulations" Microporous and Mesoporous Material 174 (2013) 126-134.

3. T. Chokbunpiam, R. Chanajaree, T. Remsungnen, O. Saengsawang, S. Fritzsche, C. Chmelik, J. Caro, W. Janke and S. Hannongbua "N<sub>2</sub> in ZIF-8: Sorbate induced structural changes and self-diffusion" Microporous and Mesoporous Material, 187 (2013) 1-6.